

2019, Australian Journal of Earth Sciences, 66 (2), 227-246

Geochemistry and provenance of the Turquoise Bluff Slate, NE Tasmania: tectonic significance

R. F. Berry^{a*}, K. Goemann^b, J. Thompson^a, S. Meffre^a and R. Bottrill^c

^aCODES and Earth Sciences, University of Tasmania, Private Bag 79, Hobart, Tas 7001, Australia;

^bCentral Science Laboratory, University of Tasmania, Private Bag 74, Tas 7001, Australia; ^cMineral Resources Tasmania, P.O. Box 56, Rosny Park, Tas 7018, Australia

Running Title: Turquoise Bluff Slate, Tasmania

* R. F. Berry ron.berry@utas.edu.au

ORCID <https://orcid.org/0000-0002-5547-3396>

Received 22 June 2018; accepted 19 October 2018

Abstract

The Ordovician Turquoise Bluff Slate in northeastern Tasmania is a two km thick sequence of deep-marine siliceous black slates. It is dominated by meta-siltstones with bimodal grain-size distributions typical of turbidite T_{E1, 2} facies. The slates have high SiO₂ indicating they are hemipelagites. The high Ba and V indicates they were deposited in an anoxic environment associated with high oceanic productivity. All these features are common in muddy turbidites.

U–Th–Pb dating of detrital monazite and authigenic xenotime in the slates supports previous evidence that the dominant cleavage, in this unit, formed during the Benambran Orogeny.

The whole-rock composition of the slates is similar to black slates in the Adaminaby Group, NSW. A review of Paleozoic whole-rock compositions from the Lachlan Orogen confirms they all have trace element contents similar to average Australian shale. However, there are subtle differences in composition. The Turquoise Bluff Slate and other Mathinna Supergroup rocks from the Eastern Tasmania Terrane have higher average Cr content than similar age turbidites from Victoria and NSW. This probably reflects a small contribution from Tasmania Cambrian ultramafic rocks in the provenance. If this were correct, northeastern Tasmania was closer to Western Tasmania in the Paleozoic than other provinces of the Lachlan Orogen, southeastern Australia. Other subtle features of the whole-rock composition of Paleozoic sedimentary rocks from the Lachlan Orogen indicate it may be possible to recognise provincial variations in composition that will provide new constraints on tectonic models of southeastern Australia.

Key words: Mathinna Supergroup, Benambran Orogeny, xenotime, whole-rock geochemistry, hemipelagic, muddy turbidite

Introduction

The Turquoise Bluff Slate (TBS) is a Middle Ordovician formation in the Mathinna Supergroup of northeastern Tasmania (Seymour, Woolward, McClenaghan, & Bottrill, 2011). The single fossil location in the TBS is regarded as Middle Ordovician (in the range Be1 [ca 476 Ma] to Da3 [ca 462 Ma]; VandenBerg in Reed, 2001). The slates are poorly exposed and very poorly studied. Previous interpretations (e.g. Seymour *et al.*, 2011) suggest this unit is more than 2.2 km thick but represents a very slowly accumulating deep-water sequence. Comparable units in Victoria such as the Bendoc Group (~700 m thick, VandenBerg, Nott, & Glen, 1992) and Mount Easton Shale (~650 m thick, VandenBerg *et al.*, 2006) are much thinner. These observations have been used as evidence by Seymour *et al.* (2011) to argue that there must be undetected structural complexity that has increased the apparent thickness of the TBS either by homogenous strain or thrust repetition.

A strong sub-horizontal cleavage in the TBS was initially considered as an early stage of the Tabberabberan Orogeny (390 Ma) associated with NE-verging folds, which was followed closely by a second steeply dipping crenulation cleavage and thrusting to the SW (Powell & Baillie, 1992). Reed (2001) argued that the early cleavage in the TBS is absent from Silurian strata nearby and is probably due to the Benambran Orogeny (ca 440 Ma); this has implications for tectonostratigraphic correlations in southeastern Australia. The apparently continuous depositional history of the Mathinna Supergroup had been a major consideration in correlating this sequence with similar age rocks in the Melbourne Zone (Powell, Baillie, Conaghan, & Turner, 1993). Seymour *et al.* (2011) further emphasised the contrast in strain history of the TBS and the overlying Panama Group (Silurian–Devonian) and mapped a possible faulted unconformity between these units. These papers have emphasised the need for a better understanding of the TBS and how it relates to other Paleozoic stratigraphy in Tasmania and across the Lachlan Orogen.

The main aims of this paper are to investigate the origin of the TBS both in terms of the sedimentary composition and the age of the dominant cleavage. The methods used include whole-rock geochemistry and microtexture analysis of the slates, for the identification of authigenic and detrital grains that can be used for mineral chemistry and U–Pb geochronology. With this data in hand, the TBS is discussed in terms of its place in the Eastern Tasmania Terrane (ETT) and in the Lachlan Orogen.

Geological setting

The Lachlan Orogen is a major part of the early Paleozoic proto-Pacific Gondwana active margin in southeastern Australia. It consists of rocks of Cambrian to early Carboniferous age whose geological history and tectonic setting has been the subject of extensive debate (e.g. Cayley, 2011; Glen, 2005). In the Ordovician, the Lachlan Orogen has two major associations: the volcanic dominated rocks of the Macquarie Arc and a more widespread quartz-rich turbidite sequence (Fergusson & Colquhoun, 2018). By the Silurian, the belt had differentiated into several major tectonic provinces (Figure 1) with different sedimentary and deformation histories, and complex unconformity relationships varying in age from Silurian to Devonian (Gray & Foster, 2004). The provenance and geochemistry of the early Paleozoic deep-marine sedimentary rocks of the Lachlan Orogen provide a context for the analysis presented here.

Tasmania is composed of a Western Tasmanian Terrane (WTT) and the ETT (Figure 1). The WTT has a basement of Proterozoic metasedimentary rocks deformed by a Cambrian arc–continent collision. After erosion in the Early Ordovician, a new cycle of shallow-marine deposition continued from the Middle Ordovician to the Early Devonian (Calver, Baillie, Banks, & Seymour, 2014; Figure 2).

In the ETT, the Ordovician to Lower Devonian succession is a thick sequence of deep-marine sandy turbidites, the Mathinna Supergroup, with strong similarities to the lower Paleozoic turbidites of the Lachlan Orogen in Victoria (Cayley, 2011; Offler & Fergusson, 2016; Powell, Baillie, & Vandenberg, 2003). No older rocks are exposed in the ETT, and the basement to the succession is unknown. The geochemistry and zircon inheritance of Devonian granites in this area indicate the basement is probably upper Neoproterozoic to Cambrian oceanic crust unlike the Proterozoic continental crust of Western Tasmania (Black *et al.*, 2010).

The Mathinna Supergroup (Figure 2) is separated into a lower Tippogoree Group and an upper Panama Group (Reed, 2001). Before 2001 these two groups were considered to be conformable but Reed (2001) argued the recumbent folding in the Tippogoree Group formed during the Benambran Orogeny (Silurian) and predated the deposition of the Panama Group. Bierlein, Foster, Gray and Davidson (2005) reported an Ar/Ar plateau age of 426.7 ± 2.4 Ma for the dominant cleavage at Lefroy in the Stoney Head Sandstone (Tippogoree Group). Recent detailed mapping demonstrated a faulted relationship between the two groups (Seymour *et al.*, 2011). These three papers supported the conclusion that the dominant cleavage in the TBS formed in the Benambran Orogeny.

The lower section of the Tippogoree Group (Seymour *et al.*, 2011) is dominated by thick, graded beds of medium to fine-grained sandstone typical of proximal turbidites (Stony Head Sandstone ~ 1 km thick). There is a fairly sharp transition at the top into the TBS. This transitional facies (Industry Road Member) at the base of the TBS has more sandy-turbidite beds than the rest of the formation. Powell *et al.* (1993) interpreted the slate as turbidite facies G (hemipelagic pelite and very fine-grained deposits of very dilute turbidity currents) but this interpretation is difficult to reconcile with the inferred thickness greater than 2.2 km for the TBS (Seymour *et al.*, 2011).

The Panama Group (Silurian–Lower Devonian) is split into four formations (Seymour *et al.*, 2011). The Yarrow Creek Mudstone is a thin-bedded grey mudstone, with minor quartz-rich siltstone beds interpreted as distal turbidites. The Retreat Formation contains medium to fine-grained quartz-rich sandstone with minor mudstone. The Lone Star Siltstone (upper Silurian) is a sequence of laminated siltstone and shale. Beds of quartz-rich sandstone become more common towards a transitional contact with the overlying Sideling Sandstone. The Lower Devonian Sideling Sandstone contains quartz-rich, fine to medium-grained sandstone with minor siltstone.

The Tabberabberan Orogeny (390 Ma; Black, McClenaghan, Korsch, Everard, & Foudoulis, 2005) occurred throughout Tasmania producing NNW-trending folds. The regional metamorphism of the Mathinna Supergroup is very low grade (anchizone: illite Kubler crystallinity index of 0.25; Patison *et al.*, 2001) and there is no change in metamorphic grade across the boundary of the TBS with the Panama Group. The most likely interpretation is that the peak metamorphic grade was reached in the Devonian and any deformation in the Silurian was at the same or lower temperature.

Voluminous granite intrusions in northeast Tasmania started before the Devonian deformation and continued until the early Carboniferous (Black *et al.*, 2005). Local zones of higher-grade contact metamorphism facies are common near these granites (Goscombe, McClenaghan, & Everard, 1992).

Within the exposures of TBS (Figure 3) discrete units can be identified. The Industry Road Member has been mapped as an approximately 1 km thick transitional zone. The rest of the TBS outcrops can be split into three domains based on the radiometric image. The TBS is relatively dark on radiometric images (Figure 3) but there is a brighter zone (RBZ) in the middle of the upper member (Seymour *et al.*, 2011). The RBZ appears to follow a path parallel to bedding and based on this interpretation a speculative fold pattern is shown. Within this pattern it is difficult to identify potential sites for large-scale thrust repetition that would explain the high apparent thickness of the formation but one

possibility discussed below is adjacent to a magnetic anomaly on the western side of the RBZ (Figure 3).

Methods

Slates of Ordovician age were collected from the Pipers River, Retreat and Georgetown area (Figure 3). The main target was the TBS, but a few samples from the underlying Stoney Head Sandstone, and the overlying Yarrow Creek Mudstone and Retreat Formation were included for comparison. All samples were collected from road cuttings but were selected to be the least weathered available. Sandstones are rare in the TBS so the program here concentrated on the dominant slate facies.

There are 180 whole-rock geochemical analyses of the Mathinna Supergroup available in the Minerals Resources Tasmania (MRT) database (<http://www.mrt.tas.gov.au/portal/samples-and-geochemistry-search>). Most of the analyses were first reported in Worthing and Woolward (2010) and Seymour *et al.* (2011). In addition, there are 22 partial analyses of the Stoney Head Sandstone reported in Purvis (1999). There were no previous analyses of the TBS in any of the data sources uncovered during this study.

Whole-rock geochemistry is publicly available for other parts of the Lachlan Orogen. The recent synthesis by Offler and Fergusson (2016) contains 37 analyses of Ordovician sandstones and mudstones from NSW (Adaminaby Group) and the Tabberabera zone of Victoria (Figure 1). Wyborn and Chappell (1983) reported 26 analyses from the Ordovician and Silurian of the Adaminaby Group. Bull and Large (2014) reported 90 analyses from the Castlemaine Group, Bendigo Zone. The Ozchem 2007 database (Sedgmen, Hazell, Budd, & Champion, 2007) contains 61 analyses of sedimentary rocks from the Castlemaine Group, Bendigo Zone and 35 analyses from the Siluro-Devonian sedimentary rocks of the Melbourne Zone (Figure 1). Together these studies provide 470 whole-rock analyses covering a large portion of the Lachlan Orogen.

Sample preparation and analysis

Seventeen slates were ground to powder in a tungsten carbide ring mill. Lithium borate fused discs and pressed powder pills were prepared and analysed for major and trace elements by XRF. Loss on ignition (LOI) was determined from 2 g of sample heated at 1000 °C for 12 hours. Analytical results and detection limits are presented in Supplementary papers (Table 1). The samples are from across the Ordovician stratigraphy and two overlying Silurian formations. The regional distribution (Figure 3) was limited by available exposures. The two Stoney Head Sandstone samples include a grey slate and a very fine-grained sandstone from the top of a turbidite unit. The TBS samples were all black slates. Two pink grey siltstone samples were collected from the Yarrow Creek Mudstone. Finally, two black slate samples from the Retreat Formation are the youngest rocks analysed in this study.

Eight samples from the TBS were selected for mineralogical analysis. At this grain size, thin sections are not effective, and the texture and mineralogy were investigated using scanning electron microscope (SEM) methods. For each sample, a 2 cm rock chip was encased in a 2.5 cm round epoxy mount, polished and carbon-coated. Automated mineral analysis (Gu, 2003) was used to locate grains of zircon, monazite and xenotime using a FEI MLA 650 scanning electron microscope (SEM) with a combination of backscattered electron (BSE) mapping to find high mean atomic number grains and energy dispersive X-ray spectroscopy (EDS) to identify grains of interest (Sack *et al.*, 2011). With this method a sample (4 cm²) can be completely scanned, with all zircon, monazite, xenotime and pyrite grains larger than 10 µm located. The rare phase search indicated that all eight samples contained these minerals.

Zircon grains were recovered by panning from 3 samples, mounted on resin and analysed by laser-ablation induction-coupled-plasma mass spectrometry (LA-ICP-MS). Initially conventional panning techniques were used to separate the zircons. However, due to the fine-grained nature of the rocks very few zircons were recovered. Instead, zircons were panned from 20 g of powdered material using a 100 mm diameter watch glass. This allowed the recovery of 20–25 μm crystals, large enough for LA-ICP-MS analysis. Monazite and xenotime grains from several samples were analysed *in situ* on the polished blocks by electron probe microanalysis (EPMA) and LA-ICP-MS.

For each of the samples selected zircon (3 samples), monazite (1 sample) and xenotime (5 samples) grains were analysed by LA-ICP-MS. The analyses were carried out using a Resonetics (now ASI) Resolution S-155 ablation system with a Coherent Compex Pro 110 excimer laser operating with ArF to produce wavelength at 193 nm and a pulse width of ~ 20 ns. All ablations were performed in a He atmosphere and the He gas was blended with Ar immediately outside the sample chamber (Eggins, Kinsley, & Shelley, 1998; Jackson, Pearson, Griffin, & Belousova, 2004). Approximately 1.6 mL/min N_2 gas was also added after the ablation cell to increase instrument sensitivity. Laser analytical parameters were similar to those described by Halpin *et al.* (2014) and are listed with a full table of measured ratios for zircon, monazite and xenotime in the Supplementary papers (Table 2). Error propagation was as described in Thompson, Meffre and Danyushevsky (2018). Uncertainties for individual analyses as quoted in tables and as error bars on U–Pb plots have been calculated to the one-sigma level. Weighted mean and intercept ages are reported at 95% confidence limits.

Zircon and monazite grains detected in the BSE images all pre-date the cleavage and have typical detrital grain shapes. Xenotime grains included both detrital and authigenic grains (see below). Electron probe micro-analysis (EPMA) concentrated on the xenotime grains and in particular on authigenic xenotime grains. Two types of EPMA analysis were carried out: the initial analysis was a general multi-element scan (26 elements) and a second round of analyses were targeted at chemical U–Th–Pb dating (Montel *et al.*, 2018) of the authigenic grains.

Polished thin sections were coated with 20 nm of carbon using a Ladd 40000 carbon evaporator. EPMA was conducted at the Central Science Laboratory, University of Tasmania, on a JEOL JXA-8530F Plus instrument equipped with 5 wavelength-dispersive x-ray spectrometers at 16 kV accelerating voltage, 80 nA beam current, and 2 μm beam diameter. The “Probe For EPMA” software package by Probe Software Inc. (Eugene, OR, USA) was used for data acquisition and quantification with the default matrix correction algorithms (Armstrong/Love Scott, LINEMU). For chemical U–Th–Pb dating, the U, Th, and Pb background intensity was determined by fitting an exponential curve to multiple background measurements on both sides of the peak (Jercinovic, Williams, Allaz, & Donovan, 2012). For all other elements a mean atomic number background correction was performed (Donovan & Tingle, 1996) that involves using calibration curves acquired on standard reference materials instead of actually measuring background intensities. A range of spectral interference corrections were applied as part of the matrix correction procedure (Donovan, Snyder, & Rivers, 1993). All elements were acquired in differential PHA mode to minimise high-order spectral interferences. Detailed conditions for both types of analysis are given in Supplementary papers (Table 3).

Results

Provenance

The automated mineral analysis identified the authigenic minerals pyrite, Fe oxide, and REE carbonate (?synchysite). Common detrital minerals include zircon, monazite and rutile (Supplementary papers, Table 4). Xenotime occurs as both detrital grains that pre-date the dominant cleavage based on their texture in BSE maps and authigenic grains that form as pressure shadows on

detrital grains or overgrow the dominant cleavage. Ilmenite is a minor component in all samples and titanite was detected in TB10 and TB11.

The primary interest here is the zircon, monazite and xenotime. The typical grain size of detrital heavy minerals in these samples is 5–30 microns, in the silt range (4–63 microns). Both zircon and monazite grains have a bimodal distribution with peaks at 10 and 25 microns diameter (Figure 4). Very similar bimodal grain-size distributions have been reported from muddy turbidites e.g. T_{E-2} intervals of the Herdotus Mega-turbidite (Talling, Masson, Sumner, & Malgesini, 2012, figure 6). Krank (1984) argued that bimodal size distributions in muddy turbidites were deposited by two discrete transport mechanisms. While it is normal to measure all the grains in a sedimentary rock to support this conclusion, the metamorphic grade and strain of the TBS precludes reliable measurement of the size of the original silicate grains (quartz, illite etc.) in the silt as they have been recrystallised. Zircon and monazite are denser than quartz, so the equivalent detrital quartz grain-size range would be slightly coarser than these heavy minerals and definitely in the range of silty turbidites T_{E-1}, T_{E-2}. Turbidite muds with abundant silt content have been widely interpreted as the result of muddy turbidite flows (Stow & Bowen, 1980).

Detrital age: zircon

In situ detrital zircon is commonly euhedral (Figure 5a–c). Thus, many of these grains were formed as small grains. Previous experience (Sack *et al.*, 2011) suggests small zircons commonly have high U and are subject to radiation damage. The BSE images of the small *in-situ* grains have dark zones in BSE maps, which commonly indicate metamict damage. To partially overcome this problem, three samples were crushed and the largest zircons available were recovered. These grains showed much less evidence of metamict zones in the BSE images (Figure 5f–h). The extracted grains appear broken but have typical sizes of 25 microns indicating they all come from the larger grain population. Thirty two grains were analysed by LA-ICP-MS using a 13 micron spot size. Six grains were discarded as unsuitable for age calculation mainly due to evidence of high U and Pb loss and were discarded. The remaining 26 grains show a range of crystallisation ages from Archean to early Paleozoic (Figure 6). Five grains form a group that define the maximum depositional age of 476 ± 32 Ma. The detrital age spectra (Figure 6) show many of the features typical of a Gondwana provenance (Squire, Campbell, Allen, & Wilson, 2006). However, there is a larger proportion of 1800–1500 Ma grains than expected. These are best explained if there is also a contribution of WTT zircons (e.g. Black, Calver, Seymour, & Reed, 2004) into these sedimentary rocks but the number of analyses is too low to make a firm conclusion.

Detrital age: monazite

Monazite is a common detrital mineral in the TBS. *In situ* LA-ICP-MS U/Pb ages were measured on 17 spots for sample TB5. Six grains defined a trend compatible with a crystallisation age of 468 ± 9 Ma (Figure 7). Some of the detrital monazite grains have cracked and rehealed (Figure 8a, c, d). Thus, the age may be slightly lower than the original crystallisation age due to a small contribution from the syn-deformational micro-boudinage infills to the age. We interpret this results as a maximum age for the dominant cleavage in the TBS.

The other detrital grains mainly cluster at 500 Ma, with the oldest grain close to 900 Ma. This distribution is similar to the detrital zircon pattern reported by Black *et al.* (2004) from the Stoney Head Sandstone.

Xenotime crystallisation age

Xenotime was detected as a trace mineral in seven of the eight samples analysed using the automated mineral recognition software. There is 5–10 times more zircon grains recognised than xenotime grains, but the grain-size range is similar. Unlike zircon and monazite, the xenotime grains are not all detrital. Most detrital xenotime grains (Figure 9a, b) have overgrowths and pressure shadows of xenotime (usually with lower heavy rare earth elements as indicated by the darker tone in BSE images). Some grains have been fractured and healed (Figure 9c), while others have spongy cores (Figure 9d). In sample TB8 large metamorphic xenotime grains overgrow the cleavage (Figure 9e) while in TB1 the xenotime is mottled indicating recrystallisation (Figure 9f). We interpret these textures as evidence that xenotime grew during the deformation (pressure shadows) and continued to grow across the cleavage after deformation was complete. The grains interpreted as syn- to post-cleavage are distinctly lower in HREE (Figure 10) and have a more uniform composition than the detrital grains.

In situ LA-ICP-MS U/Pb ages were measured on 12 spots for detrital grains in sample TB5 and TB6 (Figure 11). All but one spot is consistent with the depositional age inferred from the fossil location to the north. The dominant crystallisation age is 508–480 Ma (average 490 Ma). The three older grains range back to 1400 Ma. These grains have a bias to younger ages but are consistent with the detrital zircon age spectra from the Stoney Head Sandstone (Black *et al.*, 2004).

Sample TB1 has several xenotime grains that are mottled (Figure 9f), which is interpreted here as evidence for exsolution and recrystallisation. Four spots from this sample define an intercept age of 353 ± 9 Ma. No events in north east Tasmania can be correlated with this age but it is close to the age of the youngest granites in western Tasmania (Black *et al.*, 2005).

Sample TB8 has two large xenotime grains that overgrow the cleavage (Figure 9e). Five analytical spots from these two grains, have near concordant ages and provide an intercept age of 394 ± 5 Ma. This intercept age provides a minimum estimate for the age of the dominant cleavage in the TBS. It is within error of the Tabberabberan Orogeny in Tasmania (390 Ma) but is also consistent with a Benambran Orogeny age for the cleavage.

The xenotime grains crystallised in syn-cleavage pressure shadows are too small to be analysed by the present LA-ICP-MS technology. They are typically 2–5 microns in diameter. The pressure shadow on one grain in sample TB4 is 10 microns across (Figure 9a). On this basis chemical U–Th–Pb analysis of xenotime (Supplementary papers, Table 3) was used to decide if these grains were crystallised in the Tabberabberan (390 Ma) or during the Benambran Orogeny (*ca* 440 Ma). Five analytical spots by EPMA were collected from the grain shown in Figure 9e for comparison (Figure 12). These five spots gave a chemical U–Th–Pb age of 391 ± 76 Ma, which is within error of the LA-ICP-MS age for post cleavage xenotime in this sample. Ten analyses of xenotime pressure shadow (including seven from the grain in Figure 9a) had a weighted average age of 488 ± 38 Ma. On this basis the probability that the pressure shadow grains are more than 25 Ma older than the xenotime in TB8 is 96%. Combining the minimum age constraint from U–Pb dating of xenotime in TB8 and the maximum age constraint from U–Pb dating of monazite in TB5, with this chemical U–Th–Pb xenotime date, gives a 95% confidence range for the age of the cleavage as 473 to 437 Ma.

The precision of chemical U–Th–Pb dating is poor at 400 Ma with xenotime containing 0.2 wt% U and 0.2–0.5 wt% Th, but it is sufficient to strongly support the previous arguments (Bierlein *et al.*, 2005; Reid, 2001; Seymour *et al.*, 2011) for a Silurian age (Benambran Orogeny) for the dominant cleavage in the TBS.

Whole-rock geochemistry

The seventeen samples analysed for this project are dominated by quartz and muscovite with minor chlorite. Based on the whole-rock composition, the TBS samples contain less than 1 wt% albite and 1–3 wt% chlorite. TB11 has trace levels of paragonite. Other lithologies analysed have up to 2 wt% albite and 3–11 wt% chlorite. The bulk composition of all these rocks, except the Retreat Formation, lie very close to a quartz–illite mixing line (Figure 13). They fall in the intermediate weathering intensity band on the chemical index of alteration (CIA).

The lower part of the TBS is dark on radiogenic maps (Seymour *et al.*, 2011). This low apparent K, U and Th includes the Industry Road Member. However half way through the map distribution there is a more radiogenic member. On this basis the formation was separated into four domains (Figure 2). These domains were used to organise the samples into an order (Figure 14) that reflects the distance from the base of the unit in the present outcrop distribution (Industry Road Member: 3 samples; TBS middle: 2 samples; TBS RBZ unit, 4 samples; TBS upper; 2 samples). This order may reflect the stratigraphic order of these units but there is evidence of extensive deformation and we cannot discount the possibility that the domains defined from the radiometric image are fault bounded. The clearest trend is in K_2O where the dilution effect of high biogenic silica (see below) leads to a very low K_2O across all of the TBS. The sample compositions are only slightly higher in K and Th in the RBZ and upper part of the TBS, compared to the middle and lower parts (Figure 14).

The TBS samples (including the Industry Road member) are all very SiO_2 rich (>75 wt% SiO_2). They are not typical slates (55–65 wt% SiO_2) but have compositions that trend towards and overlap with the Ordovician cherts of NSW (Bruce & Percival, 2014). The TBS slates are low in Al_2O_3 and extremely low in total Fe (Figure 14). The low (total Fe)/Al (<0.5) indicates that these rocks were not deposited in a euxinic environment (cf. Lyons & Severmann, 2006).

The TBS slates have a high Ba/Al value, which is generally taken to indicate a high paleoproductivity (Dean, Gardner, & Piper, 1997). High Ba results from barite accumulation, which is positively correlated with the primary productivity in marine sediments (Paytan & Griffith, 2007). Other features of high productivity, such as P/Ti are not anomalous. However, P retention in sediments is complex and even in anoxic conditions it can be released from the organic matter and cycled back into the ocean (Tribovillard, Algeo, Lyons, & Riboulleau, 2006).

The TBS are similar to other parts of the Mathinna Supergroup based on many minor elements (e.g. Ti, Sc, Th, La, Rb) but the Ba and V content of the TBS is much higher than typical for the Mathinna Supergroup (Figure 15a, b). V enrichment with little or no Mo enrichment is typical of anoxic environments (Tribovillard *et al.*, 2006). The dilution effect of biogenic silica is clear on a plot of Zr vs SiO_2 (Figure 15c). While sandstones show increasing concentration of zircon with increasing SiO_2 content, the TBS samples lie along a dilution line towards a biogenic end-member with no Zr and 98 wt% SiO_2 . The array of samples projects back to the normal turbidite composition at 170 ppm Zr and 70 wt% SiO_2 . Using these endmember compositions, the biogenic component of each TBS samples was calculated (Supplementary papers, Table 1) and they range from 24 to 75% biogenic component.

Hemipelagite was defined by Pickering, Stow, Watson and Hiscott (1986) as having 5–75% biogenic material with more than 40% of clastic material in the silt range. The TBS samples have a biogenic component in this range. The grain-size evidence from the zircon and monazite indicate a dominant silt size for the terrigenous component. The TBS slates have the composition and grain size of a hemipelagite.

Discussion

Regional variation in Paleozoic turbidites of the Lachlan Orogen

High Ba, high SiO₂, low Fe black slates, which have been reported from the Adaminaby Group (Late Ordovician) of NSW, are interpreted as hemipelagic sedimentary rocks (Morand, 1990). These units show many of the same features as the TBS although the Adaminaby Group samples have more extreme Ba, and higher V (Figure 14a, b). Radiolaria have been observed in the Adaminaby Group rocks and some TBS samples have small multicrystal quartz spots (Figure 16) that may be pseudomorphs after radiolaria. Cherts and associated “siliceous siltstones” are common throughout the Lower and Middle Ordovician sedimentary rocks of NSW (Bruce & Percival, 2014) but cherts in the TBS are rare.

VandenBerg (1998) noted that the Ordovician black shales of the Mornington Peninsula are very siliceous and associated with black cherts. However, these are relatively thin units in a sandstone rich sequence. Fergusson and VandenBerg (2003) reported the black shale facies of the Castlemaine Group and the Mount Easton Shale are pelitic in composition and contrasted them with the highly siliceous composition of slates in the Bendoc and Adaminaby groups. On this basis the TBS is a better chemostratigraphic correlate of the Bendoc Group than the Mount Easton Shale.

To further consider the significance of the composition of the Mathinna Supergroup it is necessary to put the composition in the context of the geochemistry of similar age rocks in southeastern Australia. In major element terms all the lower Paleozoic deep-water siliciclastic rocks of southeastern Australia are very low in CaO and come from a weathered source. The Bendigo Zone samples in the OZchem database lie on a trend lower in K (Figure 17) and distinctly higher in Al₂O₃ than samples from all other areas. However, these samples were partly weathered when collected (T. Mernagh pers. comm.). Drill-core samples from the Bendigo Zone (Bull & Large, 2014) do not show this trend.

The trace element compositions (Figure 18) of all of the sedimentary rocks, including the Mathinna Supergroup, are typical of rocks from a source with less mafic material than post-Archean-Australian-Shale (PAAS, Taylor & McLennan, 1985) and North-American-Shale-Composite (NASC, Gromet, Dymek, Haskin, & Korotev, 1984). The ETT samples lie in the middle of the range of Lachlan Orogen sedimentary rocks on the La–Th–Sc diagram (Taylor & McLennan, 1985).

However, the ETT samples have a much higher Cr content (Figure 19a) than all other turbidite samples from southeastern Australia. Turbidites from all other localities show a near linear inverse correlation with SiO₂. Three exceptions from NSW were from sandstones crushed in a Cr steel mill where it is possible that the high Cr contents are due to contamination, alternatively there is a minor source for chromite in the provenance of the Adaminaby Group but not as much as in the ETT. For the Mathinna Supergroup sandstones more than half the samples across a range of SiO₂ contents (<87 wt% SiO₂) have double the Cr content of the Victorian and NSW samples. Bracciali, Marroni, Pandolfi and Rocchi (2007) reported a similar relationship in sandstones from Corsica and suggested the elements Th, Sc and Cr can be used to discriminate Cr contribution from ultramafic rocks from mafic sources. Using their diagram (Figure 20), most Lachlan Orogen siliciclastic rocks fall along a mixing line between a mafic and a felsic source but many ETT turbidites have higher Cr contents typical of an ultramafic source.

Detrital chromite has been widely reported in the lower to middle Paleozoic sandstones of the Western Tasmania Terrane (WTT) and reaches its maximum abundance in the Pioneer Sandstone (Calver *et al.*, 2014). Whole-rock analyses of Ordovician to Devonian siliciclastic rocks in the MRT database (<http://www.mrt.tas.gov.au/portal/samples-and-geochemistry-search>) and from Allstate Explorations NL (Hills, 2004; Purvis, 1998) show the high Cr content is widespread in Ordovician to

Devonian siliciclastic rocks of the WTT (Figure 19b). The source for this Cr is the chromite derived from Cambrian ophiolitic rocks (Berry & Crawford, 1988). The high Cr content of the ETT turbidites strongly suggests derivation from a similar area with abundant ultramafic rocks. The most plausible explanation is that the WTT contributed sediments into this sequence. However, the detrital zircon age spectra from the Mathinna Supergroup show a Gondwana signature (Black *et al.*, 2005) and not the detrital zircon age spectra typical of the Proterozoic rocks in the WTT (e.g. Mulder, Halpin, & Daczko, 2015).

The high Cr signature is present in sandstone across the whole range of ages in the Mathinna Supergroup. The absence of this high Cr signature from the Bendigo Zone and Melbourne Zone sedimentary rocks suggests that the lower Paleozoic sediments in these areas were not derived from the same source as the ETT. It is likely that the NSW and Victorian sediments were deposited in an environment that was either distal from the Cambrian ophiolites relative to the ETT or that the Cambrian ophiolite component was swamped by continental Gondwana-derived sediments.

Just as the ETT turbidites have a distinctive Cr content, there are differences between the other blocks within southeastern Australia (Figure 21). The Bendigo Zone and Melbourne Zone mudstones ($\text{Al}_2\text{O}_3 > 15\%$) have a distinctively lower Nb and Th content than the other mudstone in this database. For Sc and Nb, the Tabberabbera Zone and NSW sandstones are similar to the ETT, but they are distinctively higher in Th. This gives the impression that those provinces that are closer together now are more like each other than those that are distant regardless of age. These differences are subtle. All three elements showing differences on Figure 21 are relatively low in abundance and some of the differences may be due to interlaboratory variations. A new generation of analyses with a uniform analytical protocol is needed to confirm this observation.

Environment of deposition of the Turquoise Bluff Slate

Seventy per cent of sediment delivered in rivers to the coast is mud (Talling *et al.*, 2012) and mud dominated deep-sea marine fans are common. The most conspicuous modern example is the Amazon deep-sea fan (Piper & Deptuck, 1997). Thus, the extended period of black shale deposition in the Ordovician of northeastern Tasmania is not usual. Deep-sea black shale/chert associations were especially common in the Paleozoic (Ramsay, 1973).

Mud associated with density flows (Talling *et al.*, 2012) is commonly divided into T_{E-1} , T_{E-2} , and T_{E-3} . Massive ungraded mud (T_{E-3}) is much finer than the typical grain size of the TBS. Laminated mud (T_{E-1}) and massive graded mud (T_{E-2}) include silt-size material and have the bimodal grain-size distributions apparent in the TBS. Hemipelagic mud contains a substantial component of pelagic silica as has been recognised in the TBS from the whole-rock geochemistry. In older rocks, hemipelagite is commonly homogenous with poorly defined bedding (Pickering *et al.*, 1986) that is consistent with the appearance of outcrops of the TBS.

Structure

Hemipelagic muds accumulate at 1 to 500 m/million years but rates towards the bottom of this range are most common (Shanmugam, 2016). Typical accumulation rates in muddy turbidites are 50 to 100 m/million years (Cochrane, 1990; Feng, Baohua, Wenlong, & Chenghui, 1992; Piper & Deptuck, 1997). The TBS accumulated between 470 and 440 Ma but the actual age range is unlikely to be more than 20 million years. The apparent thickness on the southern limb (Seymour *et al.*, 2011, section 10b) is over 5 km but this is unlikely to be a true thickness. The bedding cleavage angle on this section suggests there may be some strain-induced thickening but a doubling of the thickness by homogeneous shortening is unlikely. One alternative is that the section is repeated by thrusting. In the geophysical data there is a magnetic high along the base of the more radiogenic unit (RBZ) in the

middle of the TBS (Figure 2; Seymour *et al.*, 2011). This lineament is the most likely place for a thrust that splits the section into two ~2 km thick sections. With the geochemical trends there is a monotonic increase in Ba/Al up to sample TB2 (Figure 14), which is the last sample below the magnetic lineament. In this model the upper section of the TBS would represent a distal facies lacking the sandstone elements in the Industry Road Member. Unfortunately, there is little outcrop along the line of the possible thrust and testing this suggestion will be difficult.

Tectonic implications

The boundary between the WTT and ETT has long been recognised as a terrane boundary (Baillie, 1985) juxtaposing sediments deposited on an abyssal plain (ETT) with those from a continental margin (WTT), with the terranes docking in the early Silurian Benambran Orogeny (Powell & Baillie, 1992). However, the close faunal similarities between the WTT, ETT and the Melbourne zones suggest that the Silurian and Lower Devonian sedimentary rocks in these terranes were deposited within the same paleobiogeographic province (Powell *et al.*, 1993; Rickards, Hills, Banks, & MacDonald, 2002).

Reed (2001) argued the recumbent folding in the TBS formed during the Benambran Orogeny and concluded that the ETT is the southern extension of the Tabberabbera Zone. However, recent tectonic models (Fergusson & Colquhoun, 2018; Moore, Betts, & Hall, 2016; Moresi, Betts, Miller, & Cayley, 2014) argue that the Tabberabbera Zone was deposited far from the WTT. The geochemistry of the Tabberabbera Zone is compatible with these models but the composition of the ETT has a high Cr component not seen in the Tabberabbera Zone or any other northern sections of the lower Paleozoic deep-marine depositional units of southeastern Australia. In contrast the high Cr component is easily explained if the ETT were partly sourced from the WTT. At this stage no part of the Victorian stratigraphy that has been analysed has this signature. However, there are suitable rocks along the south coast of Victoria (Mornington Peninsula, Cape Liptrap) that might provide a useful test of the provincial variation in composition of the marine siliciclastic rocks of the Lachlan Orogen.

Conclusion

The TBS is composed of hemipelagite deposited as a muddy turbidite. The grain size is dominantly silt size and has a bimodal grain-sized distribution (at least for zircon and monazite). These characteristics are typical of the turbidite T_{E-1} and T_{E-2} facies. The slates contain 24–75% biogenic material, mostly SiO_2 . They are also enriched in Ba and V suggesting deposition in an anoxic zone associated with high oceanic productivity. Similar rocks have been reported from the Adaminaby Group and are probably also common in the Bendoc Group.

The TBS contains zircon, monazite and xenotime. The zircon is all detrital. The monazite is largely detrital but has been cracked and rehealed during the formation of a strong cleavage. The U–Pb monazite age of 468 ± 5 Ma is interpreted as a maximum age for the cleavage. Authigenic xenotime provides a minimum age for cleavage development of 394 ± 5 Ma. A chemical U–Th–Pb date on syn-deformation xenotime is consistent with a Benambran age (440 Ma) for the cleavage formation but is not consistent with a Tabberabberan age. This result provides strong support for the recent re-interpretation of the recumbent folding in the TBS and Stoney Head Sandstone as the first evidence for Benambran deformation in Tasmania.

The whole-rock chemistry of the Mathinna Supergroup rocks is very similar to Paleozoic deep-marine sedimentary rocks from other domains in the Lachlan Orogen. All these rocks have typical turbidite compositions and are close to the composition of post-Archean Australian Shale. However, there are subtle regional differences that only become apparent when the composition are directly compared.

The ETT has higher Cr content than any other domain. We argue this indicates the WTT was part of their provenance even though the detrital zircon population is dominated by a well-mixed distant Gondwana source. There is evidence that the Bendigo Zone has lower Th and Nb than other provinces. The Bega Narooma Zone has higher Th in sandstone. A chemostratigraphic analysis of these rocks may provide valuable information of minor variations in the provenance and be a useful test of tectonic models that propose large-scale translations between the various provinces.

Acknowledgements

We thank Terry Mernagh and David Champion for help with background information on the analyses sourced from the OZchem database, and Michael Bruce and Robin Offler for their constructive reviews, which improved the paper. This paper is published with the permission of the Director of Mines, Tasmania.

Funding

The paper was partly supported by ARC Linkage LP160100483 Ore deposits and tectonic evolution of the Lachlan Orogen, SE Australia, and partly by the ARC Research Hub for Transforming the Mining Value Chain (project number IH130200004).

Supplementary papers

Table 1. Whole-rock XRF results, methods and sample locations.

Table 2. LA-ICP-MS methods and results.

Table 3. EPMA xenotime analyses.

Table 4. Detrital mineral abundance.

References

- Baillie, P. W. (1985). A Paleozoic suture in eastern Gondwanaland. *Tectonics*, *4*, 653–660.
- Berry, R. F., & Crawford, A. J. (1988). The tectonic significance of Cambrian allochthonous mafic–ultramafic complexes in Tasmania. *Australian Journal of Earth Sciences*, *35*, 523–533.
- Bierlein, F. P., Foster, D. A., Gray, D. R., & Davidson, G. J. (2005). Timing of orogenic gold mineralisation in northeastern Tasmania: implications for the tectonic and metallogenic evolution of Palaeozoic SE Australia. *Mineralium Deposita*, *39*, 890–903.
- Black, L. P., Calver, C. R., Seymour, D. B., & Reed, A. (2004). SHRIMP U–Pb detrital zircon ages from Proterozoic and Early Palaeozoic sandstones and their bearing on the early geological history of Tasmania. *Australian Journal of Earth Sciences*, *51*, 885–900.
- Black, L. P., McClenaghan, M. P., Korsch, R. J., Everard, J. L., & Foudoulis, C. (2005). The significance of Devonian–Carboniferous igneous activity in Tasmania, as derived from U–Pb SHRIMP dating of zircon. *Australian Journal of Earth Sciences*, *52*, 807–829.
- Black, L. P., Everard, J. L., McClenaghan, M. P., Korsch, R. J., Calver, C. R., Fioretti, A. M., Brown, A. V., & Foudoulis, C. (2010). Controls on Devonian–Carboniferous magmatism in Tasmania, based on inherited zircon age patterns, Sr, Nd and Pb isotopes, and major and trace element geochemistry. *Australian Journal of Earth Sciences*, *57*, 933–968.
- Bracciali, L., Marroni, M., Pandolfi, L., & Rocchi, S. (2007). Geochemistry and petrography of western Tethys Cretaceous sedimentary covers (Corsica and Northern Apennines): from source areas to

- configuration of margins. In J. Arribas, S. Critelli, & M. J. Johnsson (Eds.), *Sedimentary Provenance and Petrogenesis: Perspectives from Petrography and Geochemistry* (pp. 73–93). Boulder Co: Geological Society of America Special Paper 420.
- Bruce, M. C., & Percival, I. G. (2014). Geochemical evidence for provenance of Ordovician cherts in southeastern Australia. *Australian Journal of Earth Sciences*, *61*, 927–950.
- Bull, S. W., & Large, R. R. (2014). Setting the stage for the genesis of the giant Bendigo ore system. In G. R. T. Jenkin, P. A. J. Lusty, I. McDonald, M. P. Smith, A. J. Boyce & J. J. Wilkinson (Eds.), *Ore Deposits in an Evolving Earth* (pp. 161–187). London UK: Geological Society, London, Special Publications, 393.
- Calver, C. R., Baillie, P. W., Banks, M. R., & Seymour, D. B. (2014). Chapter 5. Ordovician–Lower Devonian successions. In K. D. Corbett, P. G. Quilty, & C. R. Calver (Eds.), *Geological Evolution of Tasmania* (pp. 241–271). Sydney NSW: Geological Society of Australia, Special Publication 24.
- Cayley, R. A. (2011). Exotic crustal block accretion to the eastern Gondwanaland margin in the Late Cambrian–Tasmania, the Selwyn Block, and implications for the Cambrian–Silurian evolution of the Ross, Delamerian, and Lachlan orogens. *Gondwana Research*, *19*, 628–649.
- Cochrane, J. R. (1990). 32. Himalayan uplift, sea level, and the record of Bengal fan sedimentation at the ODP leg 116 sites. In J. R. Cochran, D. A. V. Stow et al. (Eds.), *Proceedings of the Ocean Drilling Program, Scientific Results*, *116*, 397–414.
- Dean, W. E., Gardner, J. V., & Piper, D. Z. (1997). Inorganic geochemical indicators of glacial–interglacial changes in productivity and anoxia on the California continental margin. *Geochimica et Cosmochimica Acta*, *61*, 4507–4518.
- Donovan, J. J., & Tingle, T. N. (1996). An improved mean atomic number background correction for quantitative microanalysis. *Journal of the Microscopy Society of America*, *2*, 1–7.
- Donovan, J. J., Snyder, D. A., & Rivers, M. A. (1993). An improved interference correction for trace element analysis. *Microbeam Analysis*, *2*, 23–28.
- Eggins, S. M., Kinsley, L. P. J., & Shelley, J. M. G. (1998). Deposition and element fractionation processes during atmospheric pressure laser sampling for analysis by ICP-MS. *Applied Surface Science*, *127–129*, 278–286.
- Feng, C., Baohua, Y., Wenlong, S., & Chenghui, C. (1992). Characterization of fine-grained turbidite deposits from the South China Sea sediment cores. *Chinese Journal of Oceanology and Limnology*, *10*, 184–192.
- Fergusson, C. L., & Colquhoun, G. P. (2018). Ordovician Macquarie Arc and turbidite fan relationships, Lachlan Orogen, southeastern Australia: stratigraphic and tectonic problems. *Australian Journal of Earth Sciences*, *65*, 303–333.
- Fergusson, C. L., & VandenBerg, A. H. M. (2003). Ordovician — the development of craton derived deep-sea turbidite successions. In W. D. Birch (Ed.), *Geology of Victoria* (pp. 97–115). Melbourne Vic: Geological Society of Australia (Victoria Division) Special Publication, 23.
- Glen, R. A. (2005). The Tasmanides of eastern Australia. In A. P. M. Vaughan, P. T. Leat & R. J. Pankhurst (Eds.), *Terrane Processes at the margins of Gondwana* (pp. 23–96). London UK: Geological Society of London, Special Publication, 246.

- Goscombe, B. D., McClenaghan, M. P., & Everard, J. L. (1992). *Contact metamorphism of the Mathinna Beds and the depth of crustal residence during mega-kinking in northeast Tasmania*. Hobart Tas: Tasmania Department of Mines Unpublished Report 1992/34, 25pp. Retrieved from <http://www.mrt.tas.gov.au/portal/document-search>.
- Gray, D. R., & Foster, D. A. (2004). Tectonic evolution of the Lachlan Orogen, southeast Australia: Historical review, data synthesis and modern perspectives. *Australian Journal of Earth Sciences*, *51*, 773–817.
- Gromet, L. P., Dymek, R. F., Haskin, L. A., & Korotev, R. L. (1984). The “North American shale composite”: Its compilation, major and trace element characteristics. *Geochimica et Cosmochimica Acta*, *48*, 2469–2482.
- Gu, Y. (2003). Automated scanning electron microscope based mineral liberation analysis: An introduction to JKMRC/FEI mineral liberation analyser. *Journal Minerals Materials Characterisation Engineering*, *2*, 33–41.
- Halpin, J. A., Jensen, T., McGoldrick, P., Meffre, S., Berry, R. F., Everard, J. L., Calver, C. R., Thompson, J., Goemann, K., & Whittaker, J. M. (2014). Authigenic monazite and detrital zircon dating from the Proterozoic Rocky Cape Group, Tasmania: Links to the Belt-Purcell Supergroup, North America. *Precambrian Research*, *250*, 50–67.
- Hills, P. B. (2004). *EL 20/94 Salisbury Hill partial relinquishment report*. Unpublished report, 23 pp. Hobart Tas: Mineral Resources Tasmania Retrieved from <http://www.mrt.tas.gov.au/portal/document-search>.
- Jackson, S. E., Pearson, N. J., Griffin, W. L., & Belousova, E. A. (2004). The application of laser ablation-inductively coupled plasma-mass spectrometry to in situ U–Pb zircon geochronology. *Chemical Geology*, *211*, 47–69.
- Jercinovic, M. J., Williams, M. L., Allaz, J., & Donovan, J. J. (2012). Trace Analysis in EPMA. *IOP Conference Series: Materials Science and Engineering*, *32*, 012012.
- Krank, K. (1984). Grain-size characteristics of turbidites. *Geological Society, London, Special Publications*, *15*, 83–92.
- Ludwig, K. R. (2008). *User’s manual for Isoplot 3.70, a geochronological toolkit for Microsoft Excel*. Berkeley Ca: Berkeley Geochronology Center, Special Publication, *4*, 76 pp. Retrieved from http://www.bgc.org/isoplot_etc/isoplot.html
- Lyons, T. W., & Severmann, S. (2006). A critical look at iron paleoredox proxies: New insights from modern euxinic marine basins. *Geochimica et Cosmochimica Acta*, *70*, 5698–5722.
- Montel, J-M., Kato, T., Enami, M., Cocherie, A., Finger, F., Williams, M., & Jercinovic, M. (2018). Electron-microprobe dating of monazite: The story. *Chemical Geology*, *484*, 4–15.
- Moore, D. H., Betts, P. G., & Hall, M. (2016). Constraining the VanDieland microcontinent at the edge of East Gondwana, Australia. *Tectonophysics*, *687*, 158–179.
- Morand, V. J. (1990). High chromium and vanadium in andalusite, phengite and retrogressive margarite in contact metamorphosed Ba-rich black slate from the Abercrombie Beds, New South Wales, Australia. *Mineralogical Magazine*, *54*, 381–391.
- Moresi, L., Betts, P. G., Miller, M. S., & Cayley, R. A. (2014). Dynamics of continental accretion. *Nature*, *495*, 245–248.

- Mulder, J. A., Halpin, J. A., & Daczko, N. R. (2015). Mesoproterozoic Tasmania: Witness to the East Antarctica–Laurentia connection within Nuna. *Geology*, *43*, 759–762.
- Nesbitt, H. W., & Young, G. (1984). Prediction of some weathering trends of plutonic and volcanic rocks based on thermodynamic and kinetic considerations. *Geochimica et Cosmochimica Acta*, *48*, 1523–1534.
- Offler, R., & Fergusson, C. L. (2016). Proto-Pacific-margin source for the Ordovician turbidite submarine fan, Lachlan Orogen, southeast Australia: geochemical constraints. *Sedimentary Geology*, *334*, 53–65.
- Patison, N. L., Berry, R. F., Davidson, G. J., Taylor, B. P., Bottrill, R. S., Manzi, B., Ryba, J., & Shepherd, R. E. (2001). Regional metamorphism of the Mathinna Group, northeast Tasmania. *Australian Journal of Earth Sciences*, *48*, 281–292.
- Paytan, A., & Griffith, E. M. (2007). Marine barite: recorder of variations in ocean export productivity. *Deep Sea Research II*, *54*, 687–705.
- Pickering, K., Stow, D., Watson, M., & Hiscott, R. (1986). Deep-water facies, processes and models: A review and classification scheme for modern and ancient sediments. *Earth Science Reviews*, *23*, 75–174.
- Piper, D. J. W., & Deptuck, M. (1997). Fine-grained turbidites of the Amazon fan: facies characterization and interpretation. In R. D. Flood, D. J. W. Piper, A. Klaus, & L. C. Peterson (Eds.). *Proceedings of the Ocean Drilling Program, Scientific Results*, *155*, 79–108.
- Powell, C. McA., & Baillie, P. W. (1992). Tectonic affinity of the Mathinna Group in the Lachlan Fold Belt. *Tectonophysics*, *214*, 193–209.
- Powell, C. McA., Baillie, P. W., Conaghan, P. J., & Turner, N. J. (1993). The turbiditic mid-Palaeozoic Mathinna Group, northeast Tasmania. *Australian Journal of Earth Science*, *40*, 169–196.
- Powell, C. McA., Baillie, P. W., & VandenBerg, A. H. M. (2003). Silurian to mid-Devonian basin development of the Melbourne Zone, Lachlan Fold Belt, southeastern Australia. *Tectonophysics*, *375*, 9–36.
- Purvis, J. G. (1998). EL 31/96 “Mt Careless” Annual Report 1997/98. Allstate Explorations NL. Unpublished company report to MRT 98-4216, 107 pp. Retrieved from <http://www.mrt.tas.gov.au/portal/document-search>.
- Purvis, J. G. (1999). Lefroy EL1/95 Annual report. Allstate Explorations NL. Unpublished company report to MRT 99-4335, 114 pp. Retrieved from <http://www.mrt.tas.gov.au/portal/document-search>.
- Ramsay, A. T. S. (1973). A history of organic siliceous sediments in oceans. In N. F. Hughes (Ed.), *Organisms and Continents Through Time* (pp. 199–234). Society Economic Paleontology Mineralogy, Special Publication, 17.
- Reed, A. R. (2001). Pre-Tabberabberan deformation in eastern Tasmania: a southern extension of the Benambran Orogeny. *Australian Journal of Earth Sciences*, *48*, 785–796.
- Rickards, R. B., Hills, P. B., Banks, M. R., & MacDonald, G. (2002). The significance of a new locality for *Monograptus thomasi* (Early Devonian) southwest of Beaconsfield, Tasmania, and of the Corn Hill Formation. *Papers and Proceedings of the Royal Society of Tasmania*, *136*, 7–16.

- Sack, P. J., Berry, R. F., Meffre, S., Falloon, T. J., Gemmell, J. B., & Friedman, R. M. (2011). In situ location and U–Pb dating of small zircon grains in igneous rocks using laser ablation-inductively coupled plasma-quadrupole mass spectrometry. *Geochemistry, Geophysics, Geosystems*, *12*, Q0AA14, doi:10.1029/2010GC003405, 23 pp.
- Sedgmen, A., Hazell, M. S., Budd, A. R., & Champion, D. C. (2007). *OZCHEM National Whole Rock Geochemistry Dataset*. Canberra ACT: Commonwealth of Australia (Geoscience Australia). Retrieved from <http://www.ga.gov.au/metadata-gateway/metadata/record/65464/>
- Seymour, D. B., Woolward, I. R., McClenaghan, M. P., & Bottrill, R. S. (2011). Stratigraphic revision and re-mapping of the Mathinna Supergroup between the River Tamar and the Scottsdale Batholith, northeast Tasmania: Explanatory report for parts of the 1:25 000 scale Low Head, Tam O'Shanter, Weymouth, Retreat, Lilydale, Bridport, Bowood, Nabowla, Lisle and Patersonia map sheets. *1:25 000 Scale Digital Geological Map Series Explanatory Report*, *4*, 1–82. Retrieved from <http://www.mrt.tas.gov.au/portal/document-search>.
- Shanmugam, G. (2016). Submarine fans: a critical retrospective (1950–2015). *Journal of Palaeogeography*, *5*, 110–184.
- Squire, R., Campbell, I., Allen, C., & Wilson, C. (2006). Did the Transgondwanan Supermountain trigger the explosive radiation of animals on Earth? *Earth and Planetary Science Letters*, *250*, 116–133.
- Stow, D. A. V., & Bowen, A. J. (1980). A physical model for the transport and sorting of fine-grained sediment by turbidity currents. *Sedimentology*, *27*, 31–46.
- Talling, P. J., Masson, D. G., Sumner, E. J., & Malgesini, G. (2012). Subaqueous sediment density flows: Depositional processes and deposit types. *Sedimentology*, *59*, 1937–2003.
- Taylor, S. R., & McLennan, S. M. (1985). *The continental crust: Its composition and evolution*. Oxford, UK: Blackwell Scientific Publication, 312 p.
- Thompson, J. M., Meffre, S., & Danyushevsky, L. (2018). Impact of air, laser pulse width and fluence on U–Pb dating of zircons by LA-ICPMS. *Journal of Analytical Atomic Spectroscopy*, *33*, 221–230.
- Tribouillard, N., Algeo, T. J., Lyons, T., & Riboulleau, A. (2006). Trace metals as paleoredox and paleoproductivity proxies: An update. *Chemical Geology*, *232*, 12–32.
- VandenBerg, A. H. M. (1998). Ordovician of the Mornington Peninsula. *Geological Survey of Victoria, Unpublished Report 1998/12*, 4 pp. and maps. Melbourne, VIC: Geological Survey of Victoria.
- VandenBerg, A. H. M., Cayley, R. A., Willman, C. E., Morand, V. J., Seymon, A. R., Osborne, C. R., Taylor, D. H., Haydon, S. J., McLean, M., Quinn, C., Jackson, P., & Sandford, A. C. (2006). *Walhalla–Woods Point–Tallangalook special map area geological report*. Melbourne Vic: Geological Survey of Victoria Report 127, 449 pp.
- VandenBerg, A. H. M., Nott, R. J., & Glen, R. A. (1992). *Bendoc 1:100 000 map, geological report*. Melbourne Vic: Geological Survey of Victoria Report, 90, 122 pp.
- VandenBerg, A. H. M., Willman, C. E., Maher, S., Simons, B. A., Cayley, R. A., Taylor, D. H., Morand, V. J., Moore, D. H., & Radojkovic, A. (2000). *The Tasman fold belt system in Victoria*. Melbourne Vic: Geological Survey of Victoria Special Publication, 462 pp.
- Worthing, M. A., & Woolward, I. R. (2010). Explanatory Report for the Dublin Town (5840), Brilliant (5841), Falmouth (6040) and Beaumaris (6041) geological map sheets. *Explanatory Report 1:25*

000 Scale Digital Geological Map Series Mineral Resources Tasmania 3, 75 pp. Retrieved from <http://www.mrt.tas.gov.au/portal/document-search>.

Wyborn, L. A. I., & Chappell, B. W. (1983). Chemistry of the Ordovician and Silurian greywackes of the Snowy Mountains, southeastern Australia: an example of chemical evolution of sediments with time. *Chemical Geology*, 39, 81–92.

Figures

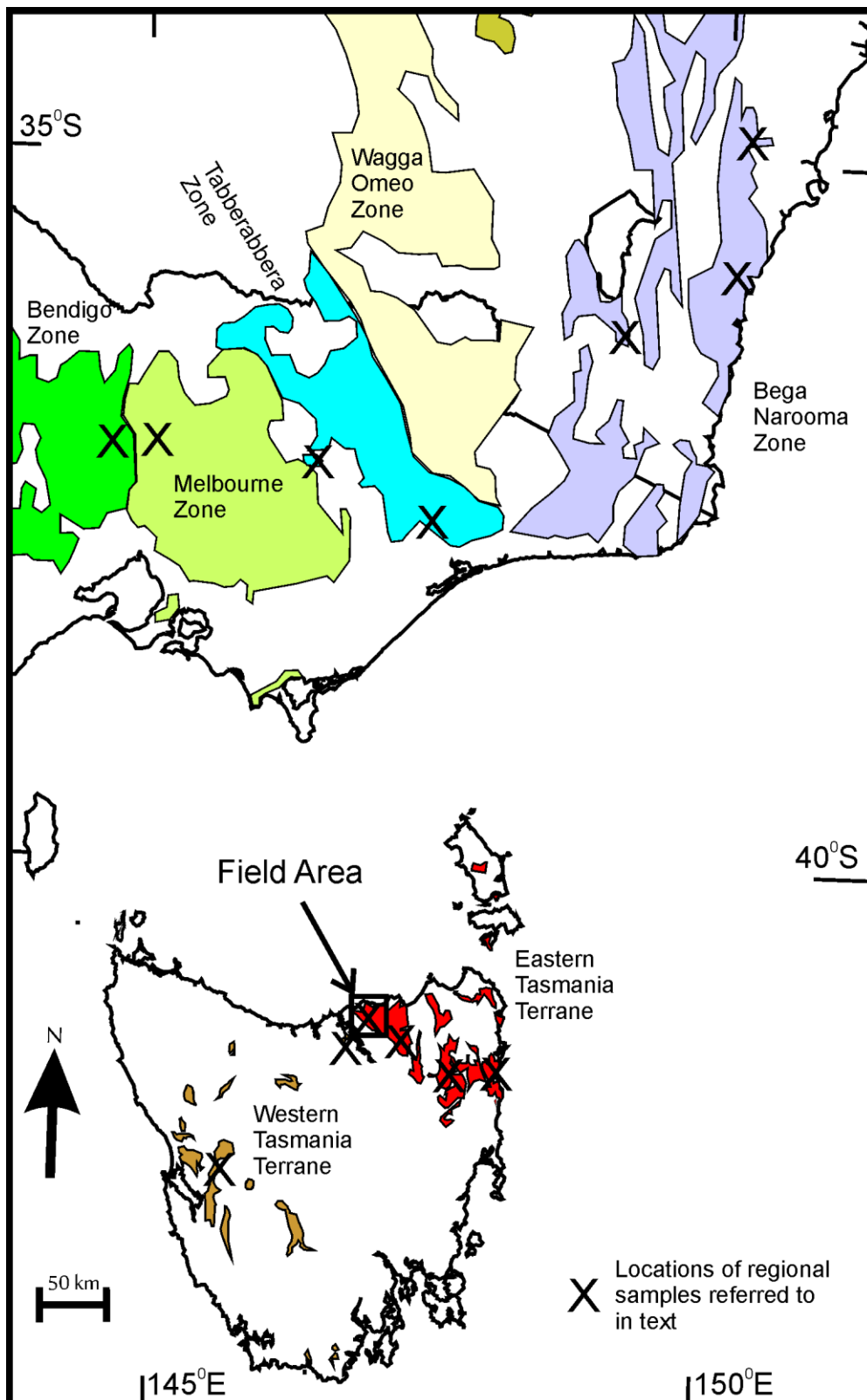


Figure 1. Regional map of southeastern Australia showing the distribution of Ordovician to Devonian sedimentary rocks in each large tectonic element (after Calver *et al.*, 2014; Offler & Fergusson, 2016). Approximate location of sedimentary rocks for which whole-rock compositions are discussed are shown as crosses.

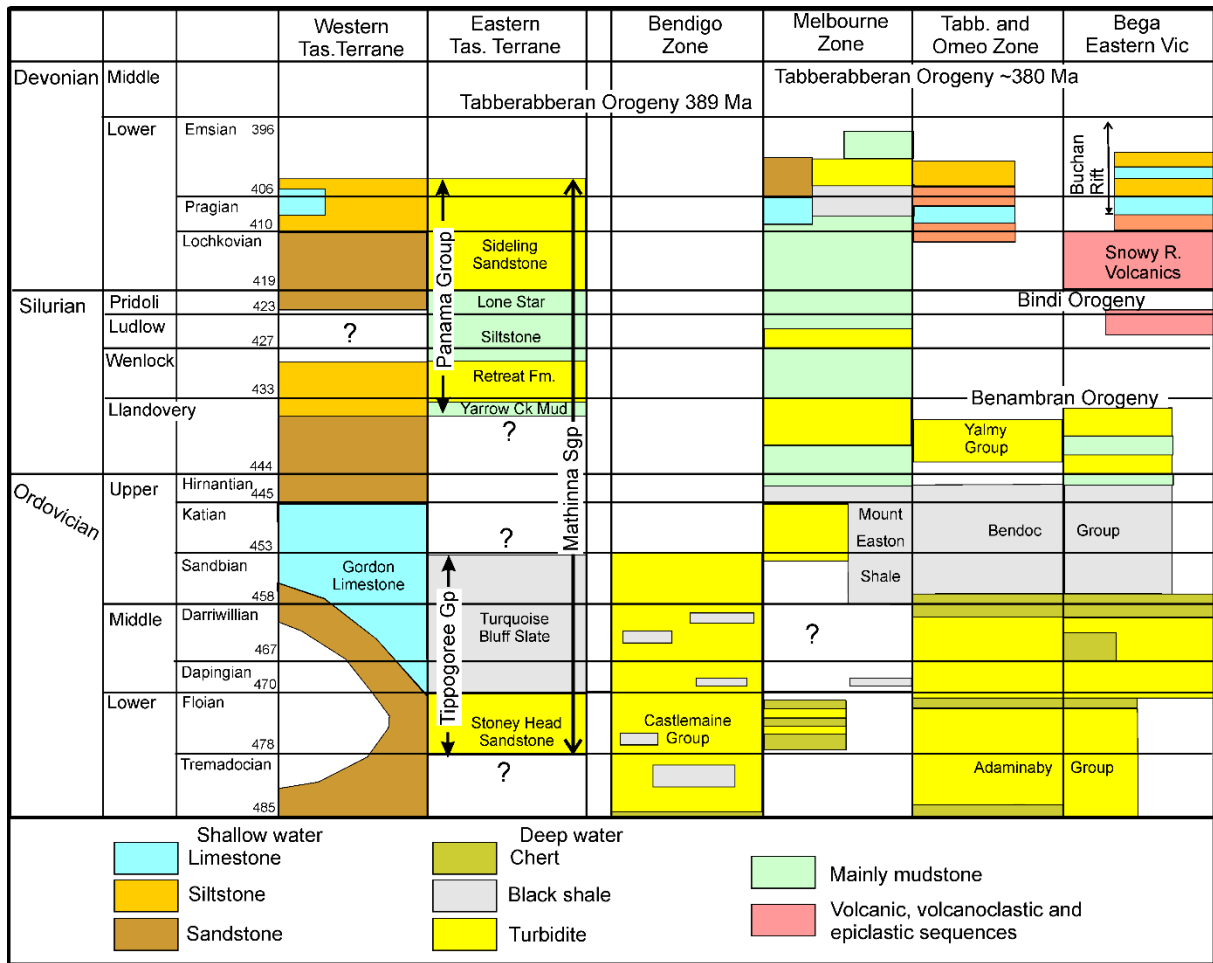


Figure 2. Comparison of Ordovician to Lower Devonian stratigraphy across southeastern Australia. Simplified from Calver *et al.* (2014), Fergusson and Colquhoun (2018), Glen (2005) and VandenBerg *et al.* (2000).

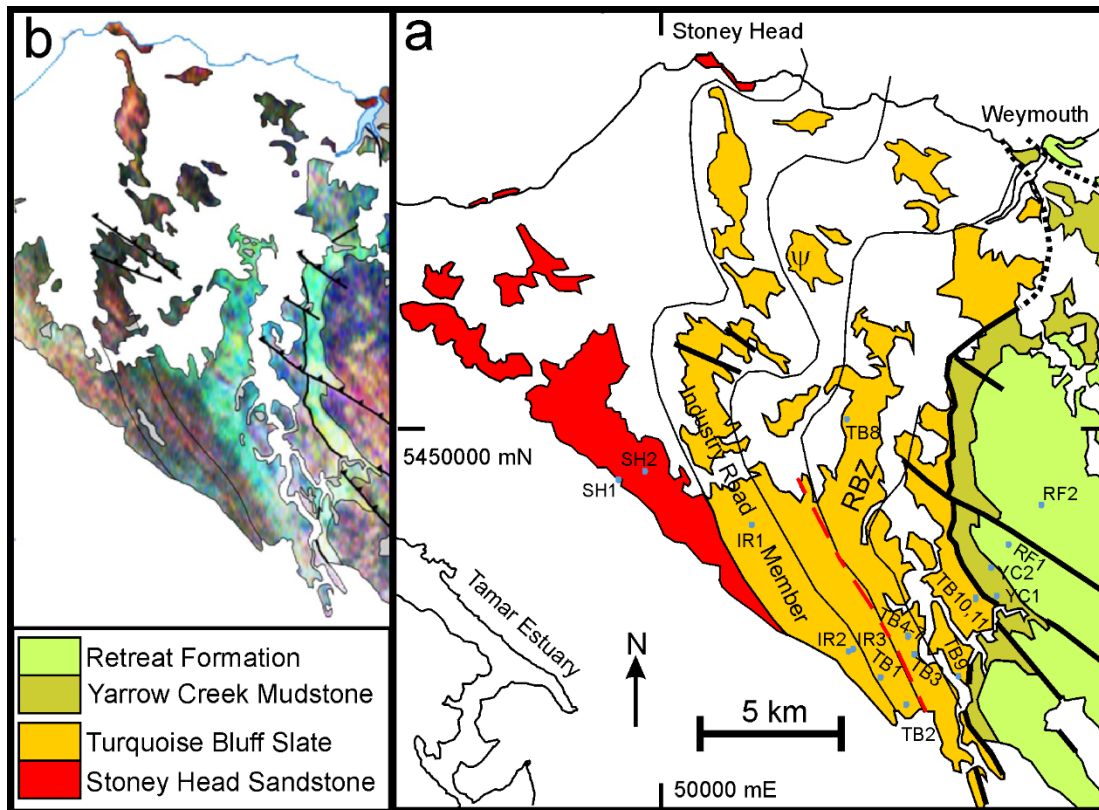


Figure 3. Georgetown–Weymouth area showing the regional distribution of Tappogoree Group and radiometric image from Seymour *et al.* (2011). (a) Geology: The TBS is sub-divided into four units partly based on brightness in radiometric image (RBZ) is radiometric bright zone visible in (b). Red dashed line is the position of magnetic lineation discussed in the text. The location of samples mentioned in the text are shown. Ordovician fossil location shown as ψ . (b) Section of radiometric image showing basis for RBZ.

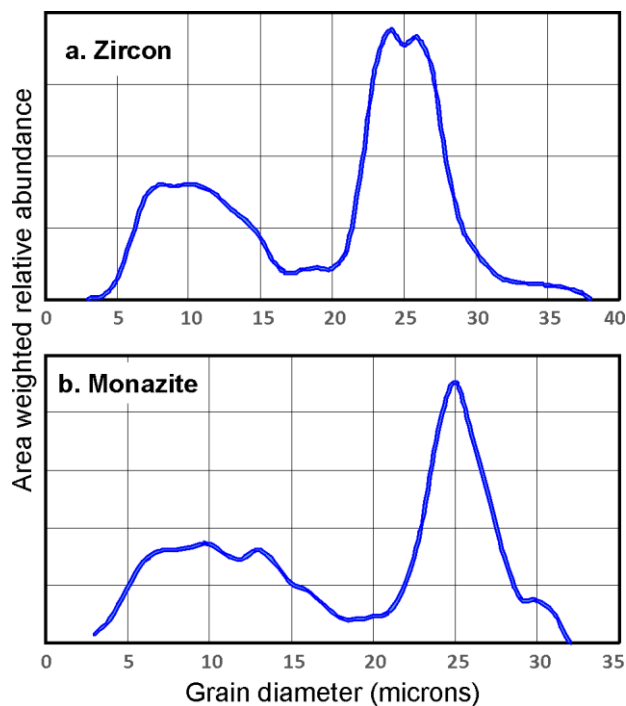


Figure 4. Area weighted grain-size (equivalent circle diameter) distribution for (a) zircon: 1064 grains and (b) monazite: 737 grains in samples from the Turquoise Bluff Slate.

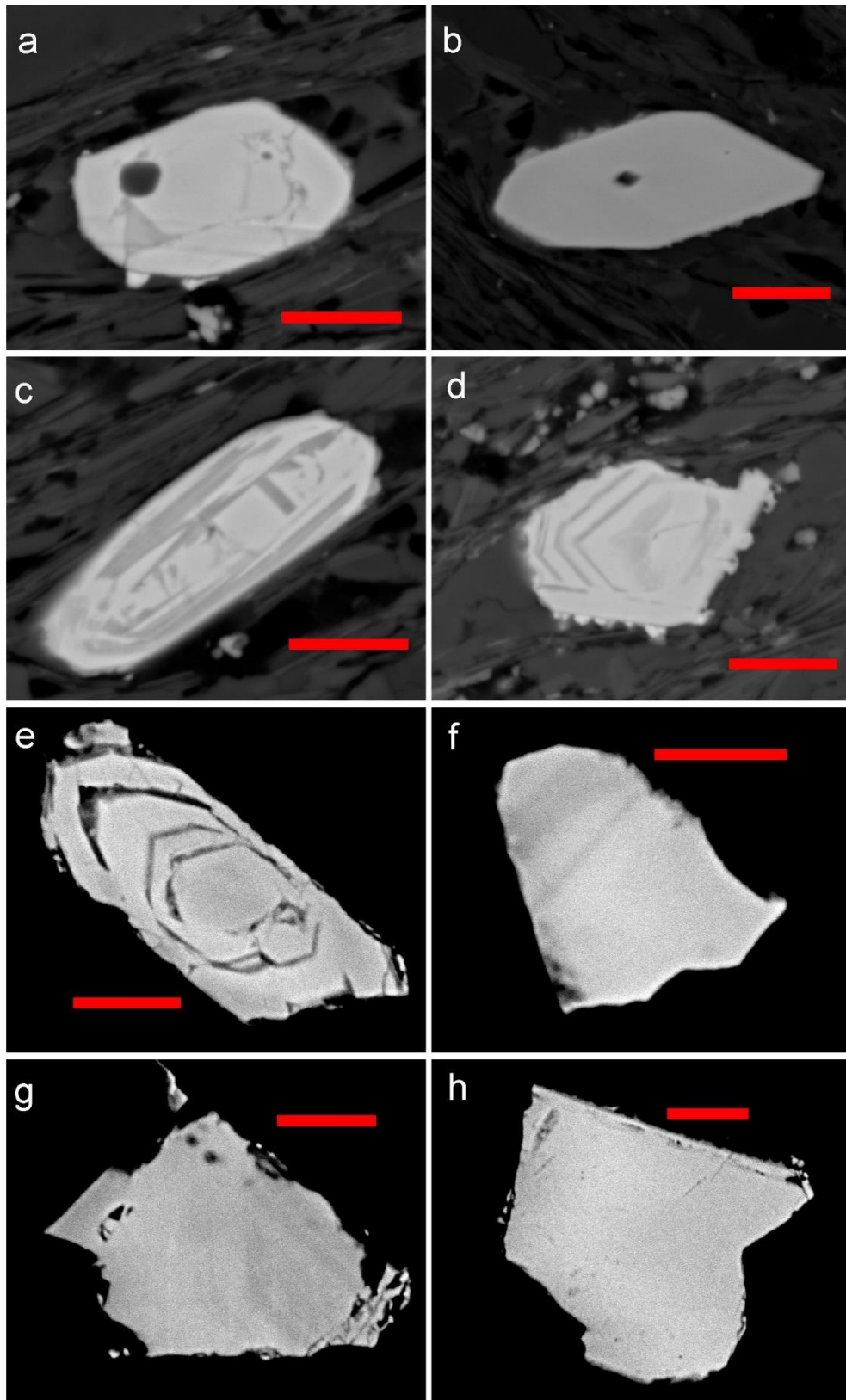


Figure 5. Detrital zircon: (a–d) *in situ* grains. Dark zones are interpreted as metamict zircon that will produce unreliable U/Pb ages; (e–h) grains recovered by heavy mineral separation. For grain (e) much of the metamict zircon has been lost during the separation process. Other grains show a more uniform BSE tone reflecting undamaged zircon. Red bar is 10 microns long on all figures.

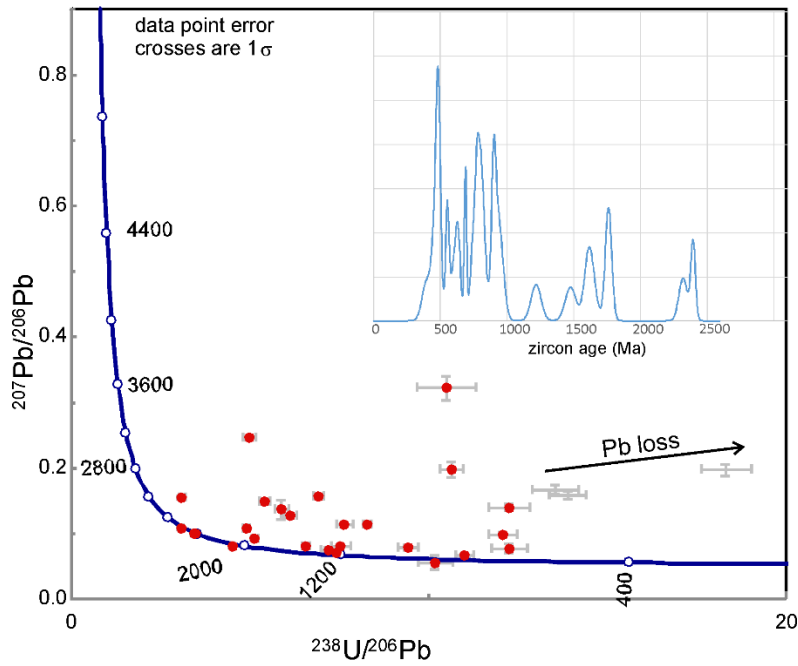


Figure 6. Inverse Concordia diagram showing location of 26 valid grains from 3 samples. Spots with red centres are included as valid analyses. Inset shows kernel density estimates of detrital zircon age distribution in TBS ($^{207}\text{Pb}/^{206}\text{Pb}$ methods for ages <1000 Ma and $^{207}\text{Pb}/^{206}\text{Pb}$ for older ages.)

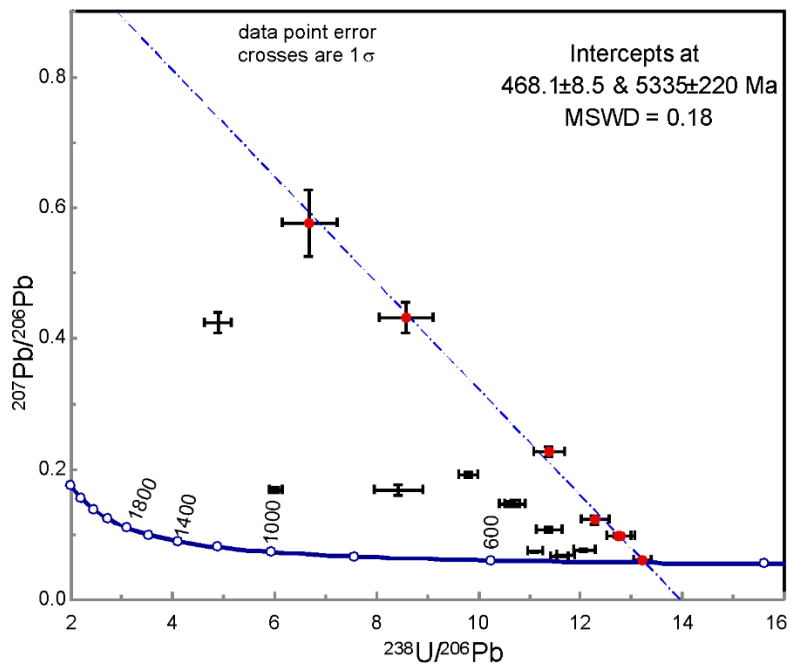


Figure 7. Inverse Concordia diagram showing composition of 17 valid spot analyses. Intercept age calculated from six youngest grains using Isoplotv4 (Ludwig, 2008)

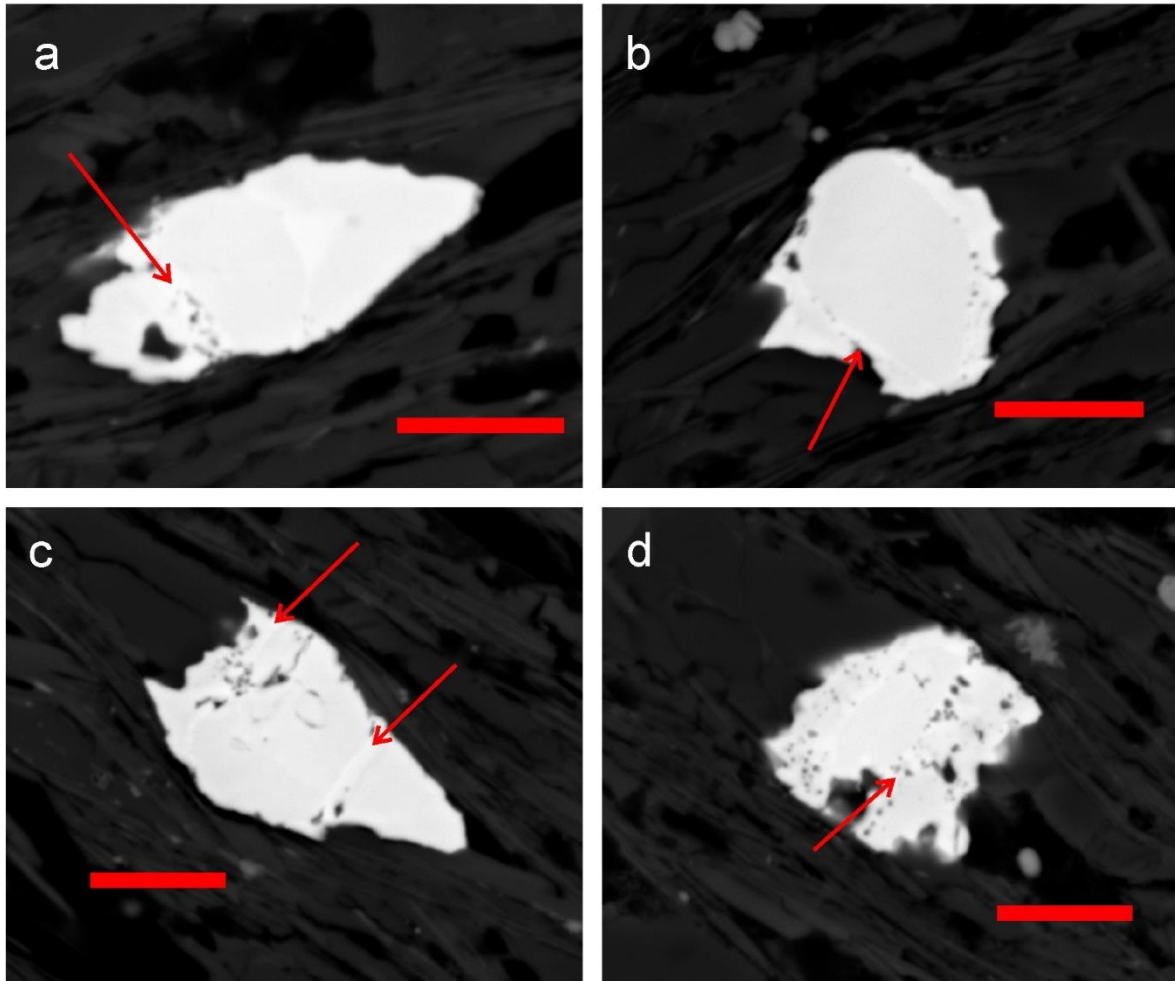


Figure 8. *In-situ* detrital monazite grains: (a) partly cracked and healed grain with monazite pressure shadow on left side, (b) detrital with monazite pressure shadows, (c) grain cracked and healed with brighter monazite, and (d) grain cracked and partially healed. Red bar is 10 microns long on all figures. Red arrows point to healed cracks and microboudinage infills.

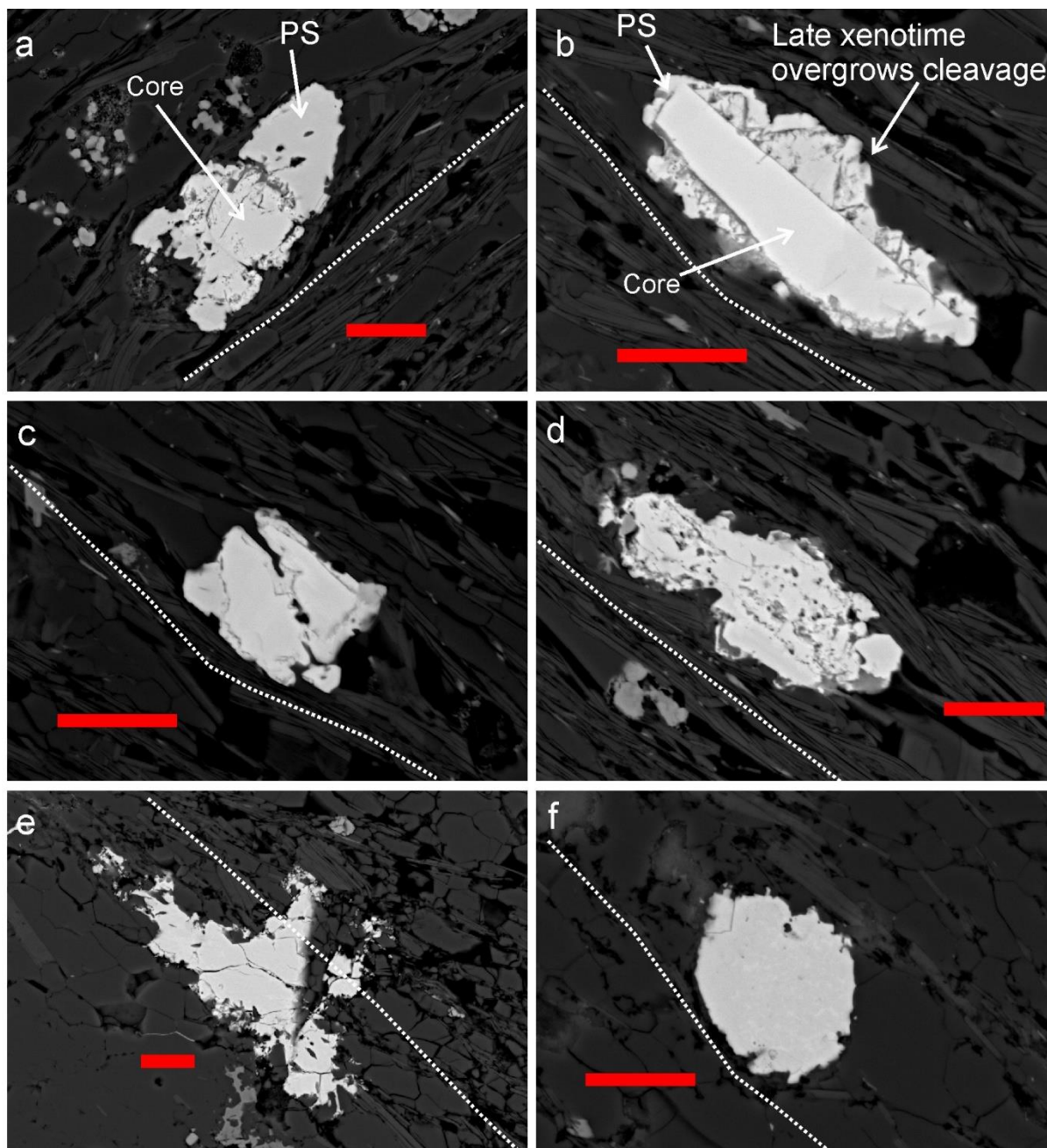


Figure 9. BSE images of xenotime grains. (a) Xenotime pressure shadow on detrital xenotime (TB4). (b) Elongate xenotime aligned in cleavage with xenotime overgrowths (TB5). There are small pressure shadows at the end of the detrital grain but most of the authigenic xenotime is along the longer side and overgrows the cleavage. (c) Cracked and rehealed detrital xenotime grain (TB5). (d) Spongy xenotime grain aligned in cleavage (TB5). (e) Large xenotime grain growing across the cleavage (post cleavage age inferred) (TB8). (f) Small xenotime with fine-scale mottling (post cleavage age measured by LA-ICP-MS) (TB1). Red bar is 10 microns long on all figures. Cleavage shown as white dotted line. PS is pressure shadow.

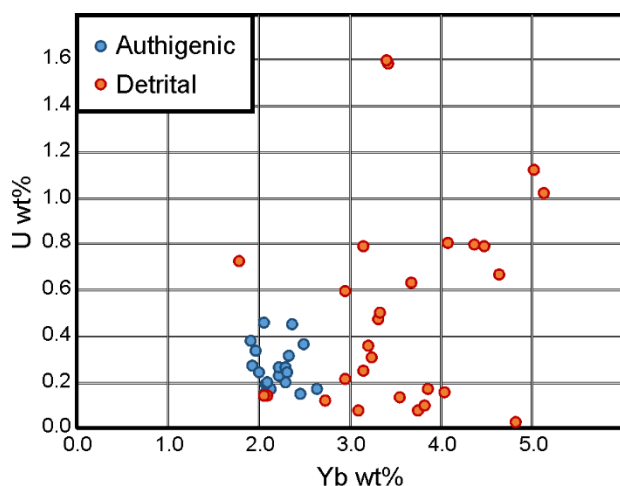


Figure 10. Comparison of the composition of detrital and authigenic xenotime grains.

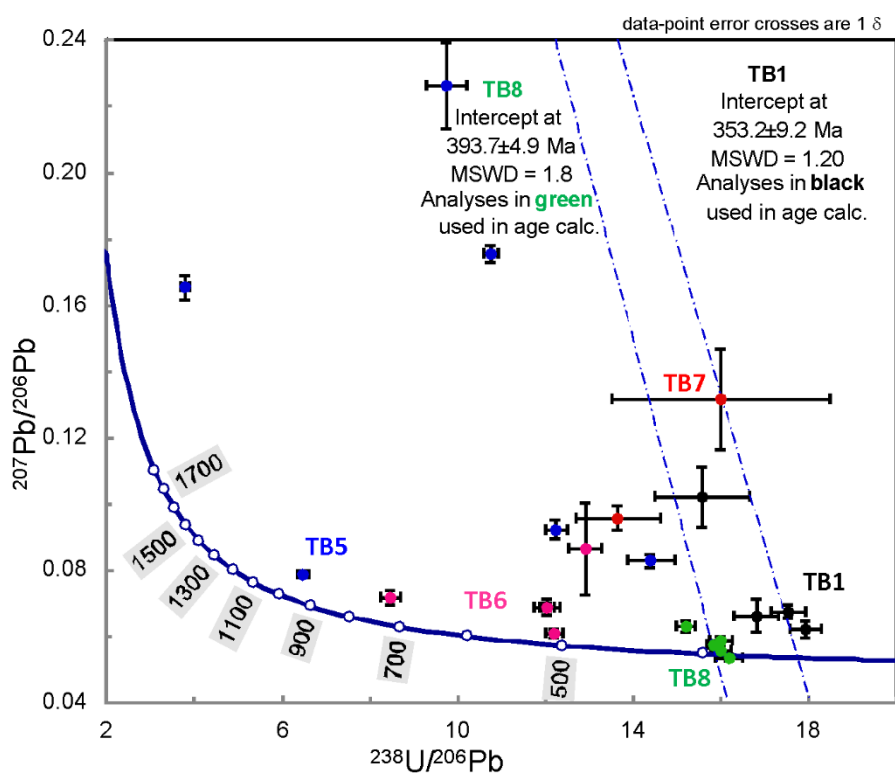


Figure 11. Inverse Concordia diagram showing U/Pb composition of 17 xenotime grains. Intercept age calculated for post cleavage grains in sample TB8 and four mottled grains in TB1. Intercept age calculated using Isoplotv4 (Ludwig, 2008)

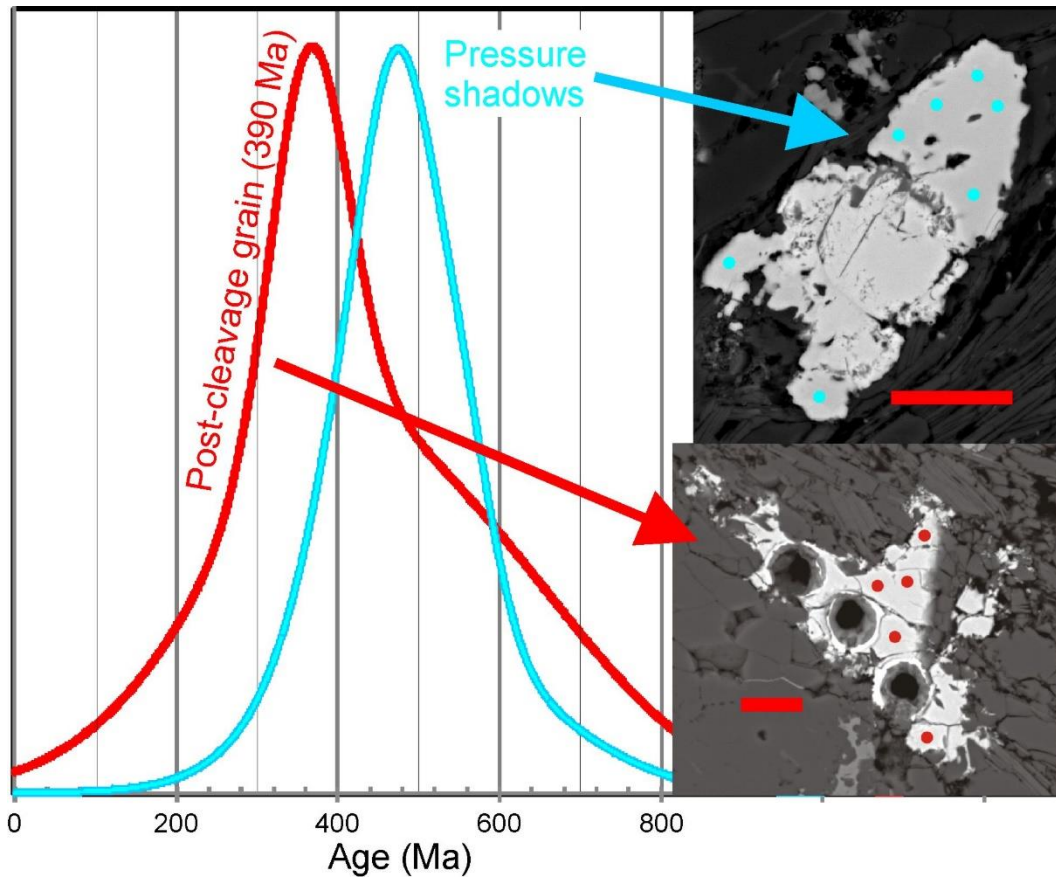


Figure 12. Kernel age distribution based on chemical U–Th–Pb ages for post-cleavage xenotime grains and pressure shadows on detrital grains. Inset pictures show position of EPMA (as 2-micron spots) and the three LA-ICP-MS analysis (of 5) holes on which the 390 Ma age of the grain was determined (see Figure 9e). Red scale bars are 10 microns long.

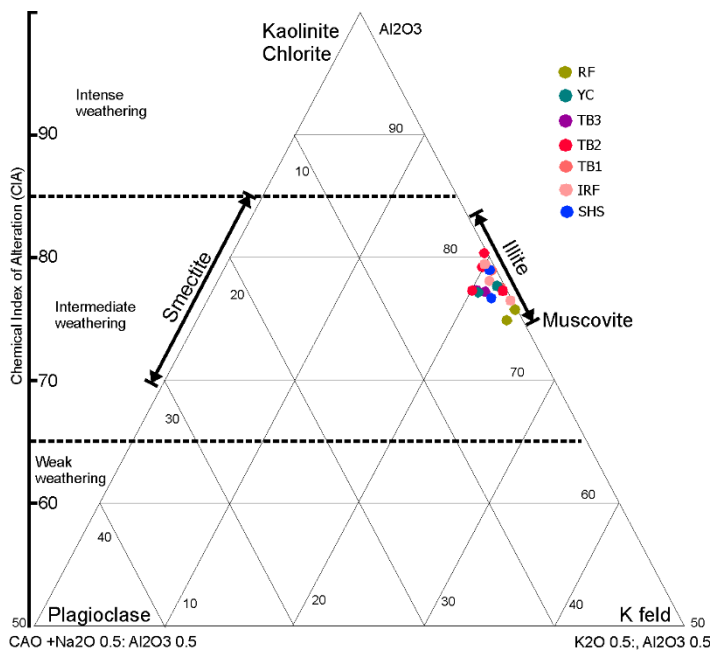


Figure 13. The A–CN–K diagram (molar Al_2O_3 – $\text{CaO}+\text{Na}_2\text{O}$ – K_2O , no carbonate correction carried out) and CIA (Chemical Index of Alteration) values for samples in this study. CIA calculated as suggested by Nesbitt and Young (1984).

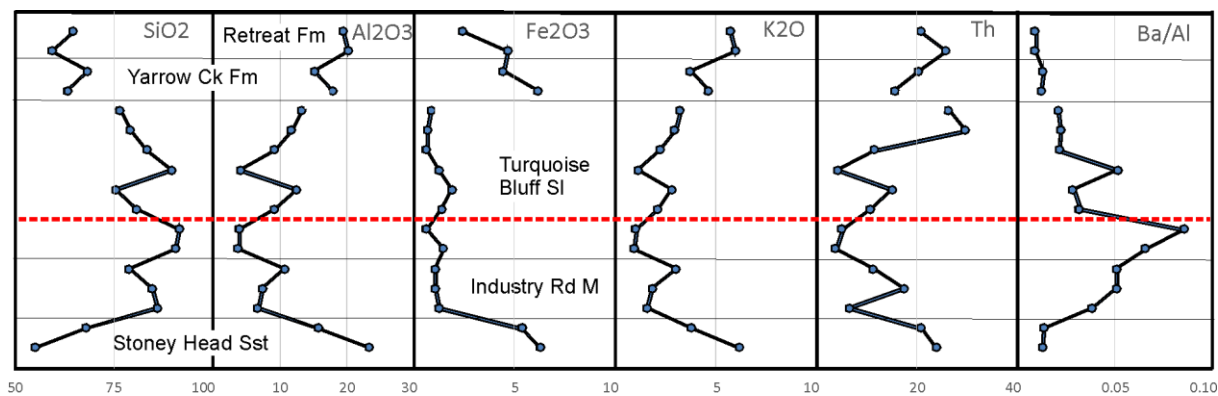


Figure 14. Slate samples arranged in approximate stratigraphic order (order of numbers on Figure 2) showing the variation of key compositional variables across the TBS. Red dashed line is position of magnetic anomaly shown on Figure 3.

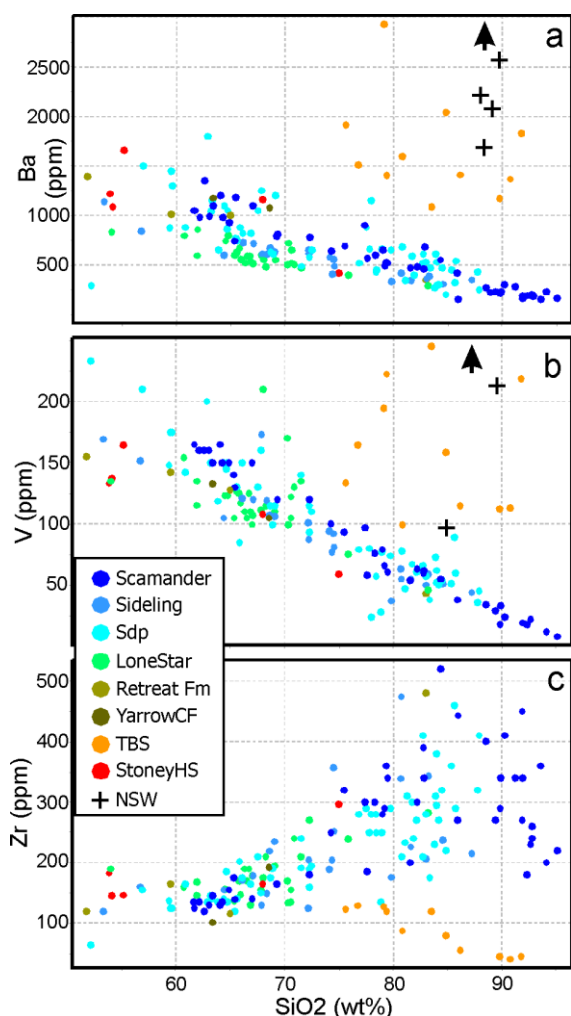


Figure 15. Comparison of trace element content of the TBS with other units in the Mathinna Group (see text for sources). Units in the legend are ordered from youngest (blue) to oldest (red). Scamander area samples and the Sideling Sandstone are Lower Devonian. Sdp samples, from near Mathinna, are mainly Silurian but may include some Devonian rocks. Lone Star Formation, Retreat Formation and Yarrow Creek Mudstone are Silurian. TBS and Stoney Head Sandstone are Ordovician. Samples labelled as NSW are black slate samples of Morand (1990) from the Adaminaby Group. Zr was not reported for these samples. Arrows indicate more NSW samples at higher Ba and V.

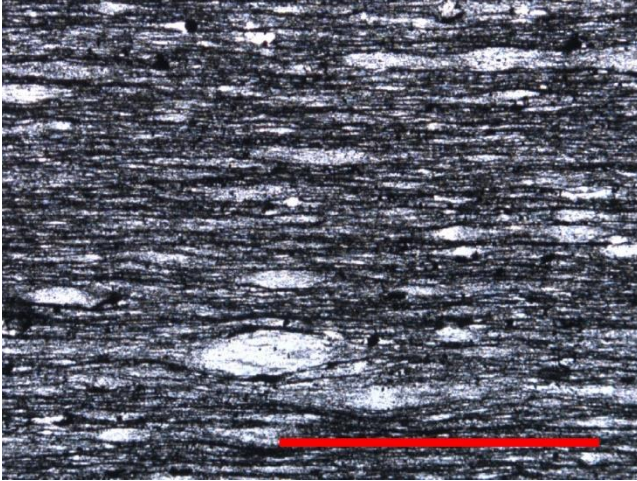


Figure 16. Photomicrograph (plane polarised transmitted light) of sample TB8 showing multicrystal quartz spots interpreted as deformed radiolarians. Red bar is 1 mm long.

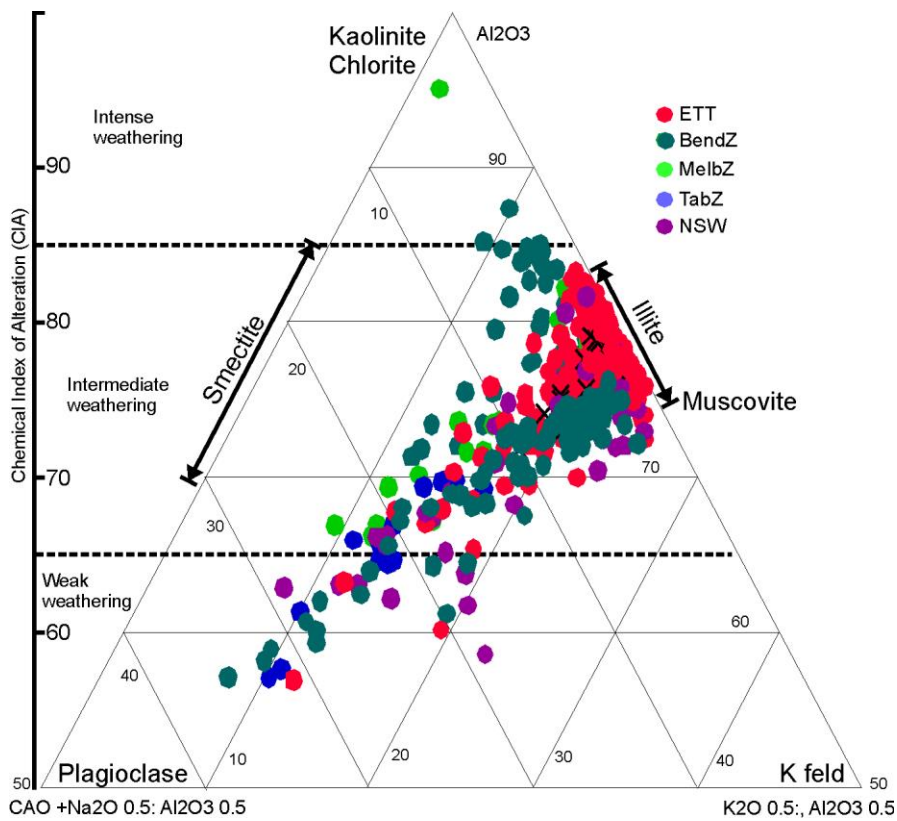


Figure 17. Molar K-CN-A diagram (Nesbitt & Young, 1984) for Lachlan Orogen turbidites.

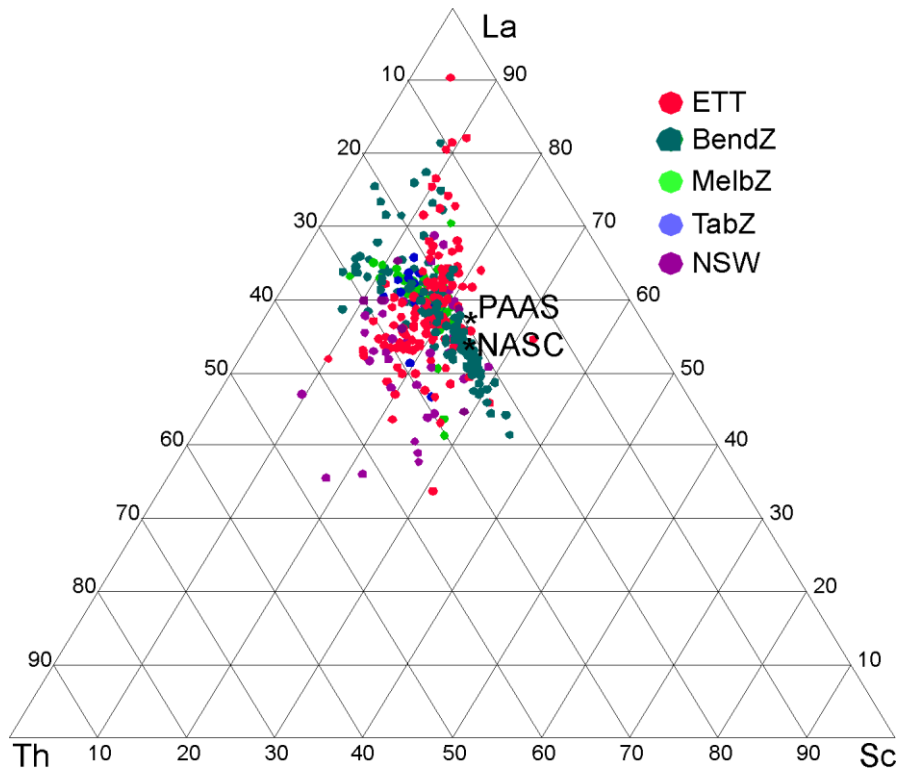


Figure 18. La–Th–Sc diagram showing the composition of Paleozoic deep-water sedimentary rocks from southeastern Australia. Composition of post-Archean-Australian-Shale (PAAS) from Taylor & McLennan (1985) and North-American-Shale-Composite (NASC) from Gromet *et al.* (1984).

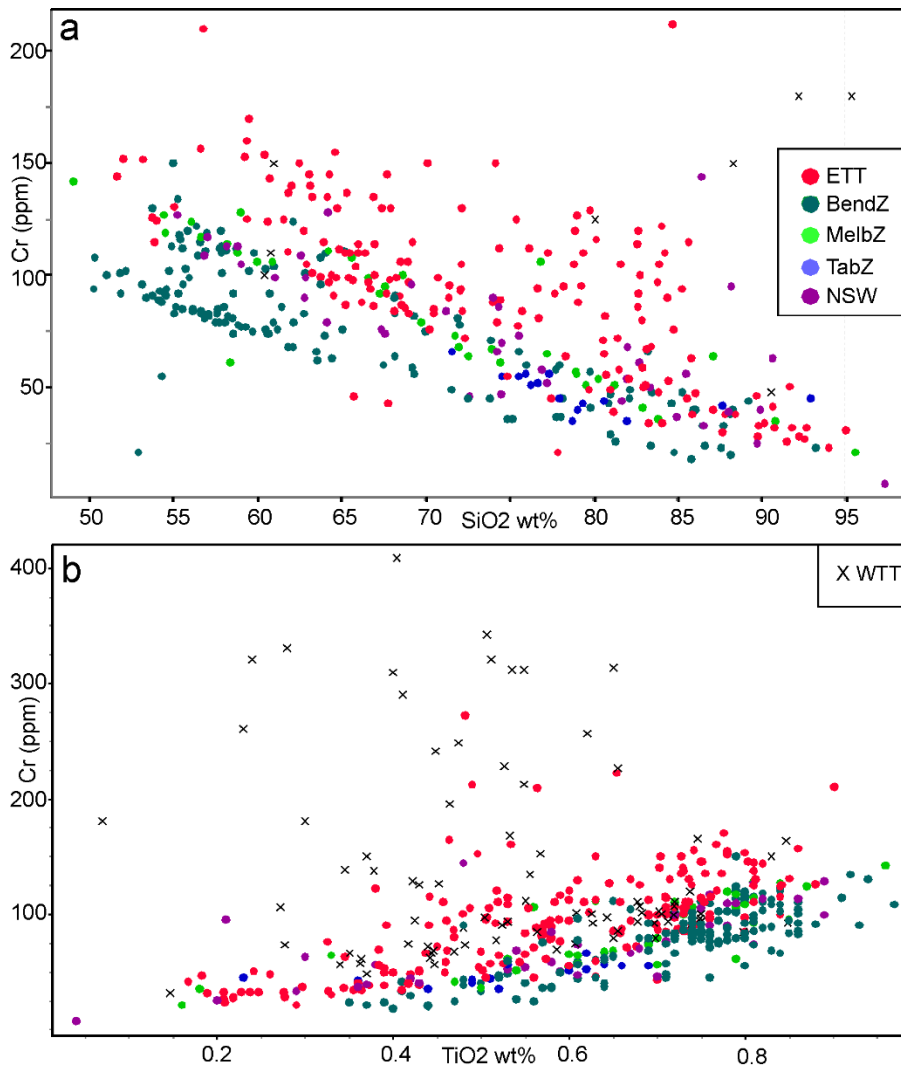


Figure 19. Plot of Cr variations in siliciclastic sequences. (a) Cr vs SiO₂ for siliciclastic rocks from the Lachlan Orogen (below 220 ppm Cr); and (b) Cr vs TiO₂ for WTT siliciclastic sequences and their comparison with Lachlan Orogen turbidites.

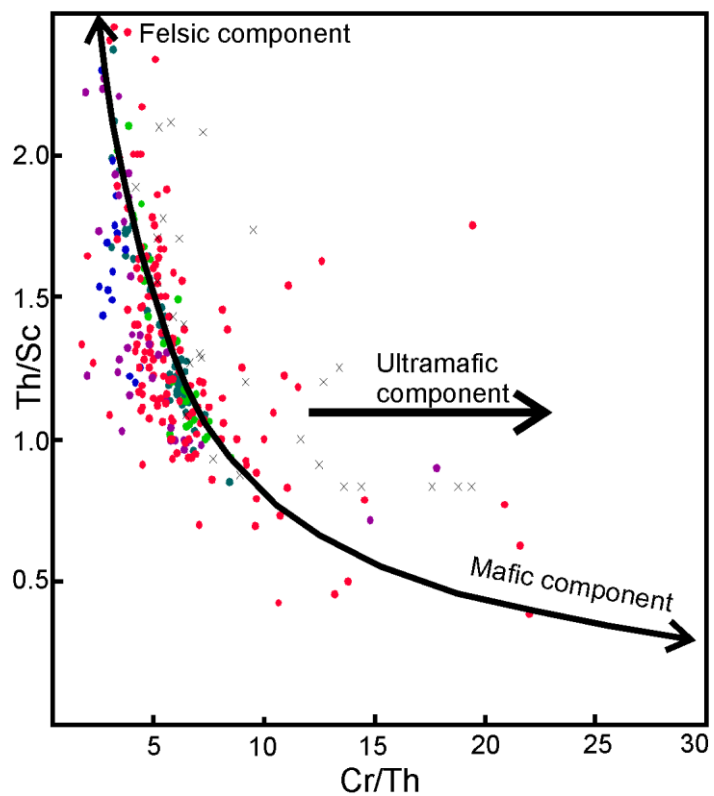


Figure 20. Lachlan Orogen siliciclastic rocks plotted on a Th/Sc versus Cr/Th diagram as suggested by Bracciali *et al.* (2007). A mixing line between mafic and felsic sources is drawn through the main data array. A contribution from an ultramafic source shifts sedimentary rocks to higher Cr/Th without changing the Th/Sc ratio. Legend for symbols is as shown in Figure 18.

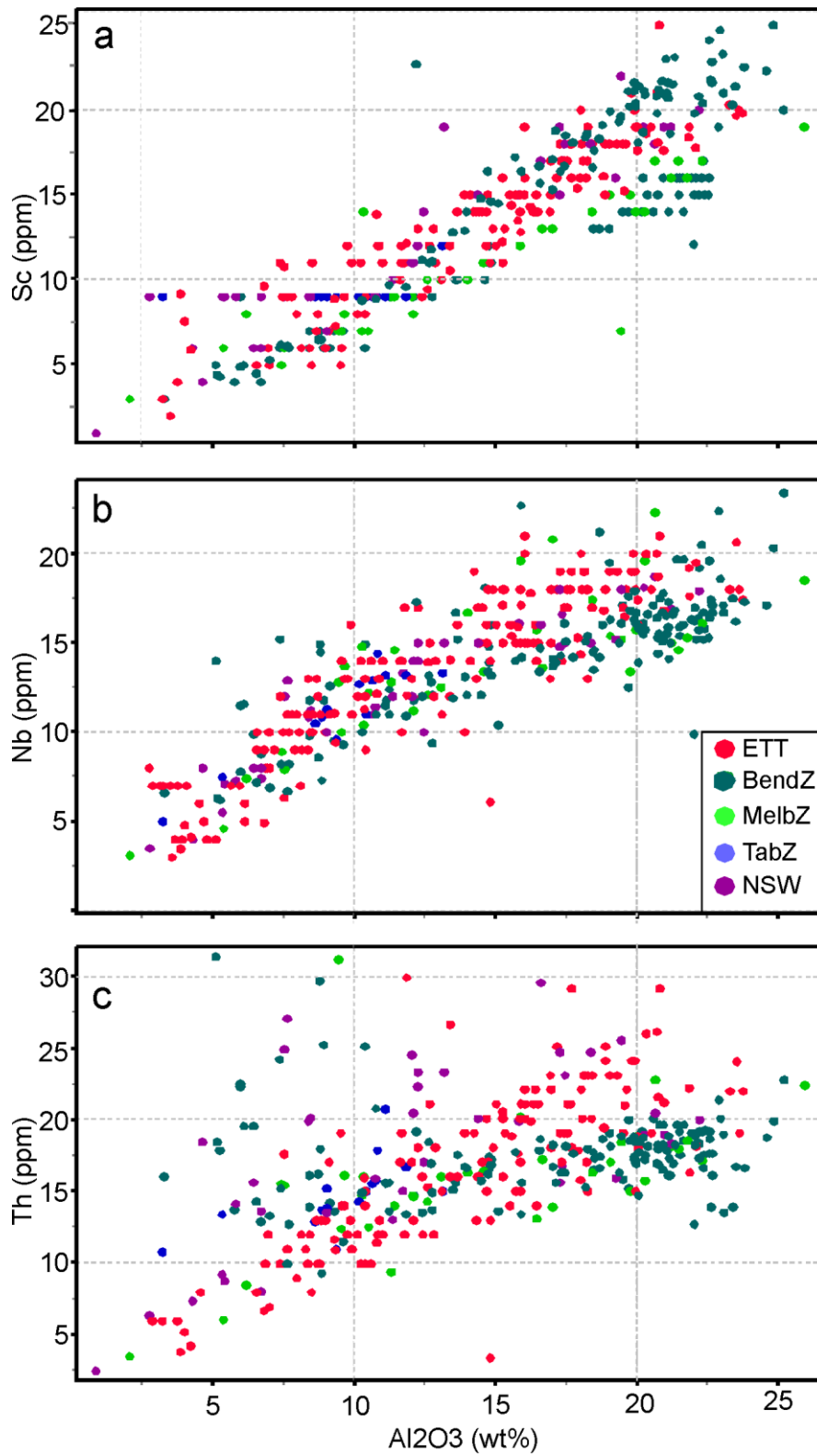


Figure 21. Sc, Nb and Th content of Lachlan Orogen siliciclastic rocks plotted against Al_2O_3 .